Available online at www.sciencedirect.com
ScienceDirect
Deep-Sea Research II 55 (2008) 1195–1217
DEEP-SEA RESEARCH PART II
www.elsevier.com/locate/dsr2

Physical and bio-optical observations of oceanic cyclones west of the island of Hawai'i

Tommy D. Dickey[a,*], Francesco Nencioli[a], Victor S. Kuwahara[a,1], Carrie Leonard[b], Wil Black[a], Yoshimi M. Rii[c], Robert R. Bidigare[c], Qin Zhang[a]

[a]*Ocean Physics Laboratory, Department of Geography, University of California, Santa Barbara, 6487 Calle Real, Suite A, Goleta, CA 93117, USA*
[b]*BAE Systems, Honolulu, HI, USA*
[c]*SOEST, Department of Oceanography, University of Hawai'i, Manoa, HI, USA*

Accepted 19 January 2008
Available online 1 May 2008

Abstract

Interdisciplinary observations of mesoscale eddies were made to the west of the island of Hawai'i. A central goal of the studies is to improve our understanding of the coupling of physical, biological, and biogeochemical processes that occur within these eddies. A specific objective was to test the hypothesis that the physical mechanisms of mesoscale eddies result in increases in nutrient availability to the euphotic layer, increases in primary production, changes in biological community compositions and size distributions, and increases in carbon flux to the deep sea. Data were obtained from ships, surface drifters, and satellite sensors during three separate field experiments. Variability was associated with two well-developed cyclonic, cold-core mesoscale eddies, Cyclone *Noah* and Cyclone *Opal*, which were observed during the E-Flux I (survey November 6–20, 2004) and E-Flux III (survey March 10–27, 2005) field campaigns, respectively. No mesoscale eddies were found during E-Flux II (survey January 10–19) when winds were erratic in magnitude and direction, supporting the hypothesis that persistent trade winds drive the production of cold-core mesoscale eddies in the lee of the Hawaiian Islands. Cold-core eddies were present in the E-Flux study area for about 2/3 of a year beginning May 1, 2004 and trade winds prevailed for about 3/4 of the same year.

Both Cyclone *Noah* and Cyclone *Opal* were generated during strong, persistent northeasterly trade wind conditions and appeared downwind of the 'Alenuihaha Channel separating the islands of Maui and Hawai'i. The likely production mechanism for both mesoscale cold-core eddies involves localized wind-stress-curl-induced upwelling produced by trade wind forcing. Cyclone *Noah* was likely spun up by strong trade winds just to the southwest of the 'Alenuihaha Channel (~20.10°N, 156.40°W) between August 13 and 21, 2004 based on MODIS satellite sea-surface temperature (SST) imagery and QuikScat satellite wind data, and apparently began to dissipate by mid-December 2004. Cyclone *Opal* was likely spun up by strong trade winds between February 2 and 18, 2005 southwest of the 'Alenuihaha Channel (~20.30°N, 156.30°W), but was no longer evident in April 2005.

Both Cyclone *Noah* and Cyclone *Opal* had strong physical, chemical, and biological expressions and displayed similar maximum tangential current speeds of ~60 cm s^{-1}. However, Cyclone *Opal* was more symmetric and larger in scale (roughly 180–200 km in diameter compared to ~160 km in horizontal scale for Cyclone *Noah*). Both mesoscale eddies displayed significant doming in their centers and in some cases outcroppings of isothermal, isopycnal, nutrient, and chlorophyll *a* isopleths. After formation and a slow drift southward, Cyclone *Noah* remained in nearly the same location (roughly 19.60°N, 156.50°W) during the 3-week in situ sampling period, whereas Cyclone *Opal* drifted southward by ~165 km over a similar time span of sampling. Interestingly, the physical manifestations of both features were relatively unchanged during the ship-based surveys; however, the biology appears to have evolved within Cyclone *Opal*. The present report sets the context for several other E-Flux studies.

Keywords: Hawai'i; Mesoscale processes; Cyclonic eddies; E-FLUX project; Physical–biological coupling

*Corresponding author. Tel.: +1 805 893 7354; fax: +1 805 967 5704.
E-mail address: tommy.dickey@opl.ucsb.edu (T.D. Dickey).
[1]Currently at Faculty of Education, Soka University, Tokyo, Japan.

0967-0645/$ - see front matter © 2008 Elsevier Ltd. All rights reserved.
doi:10.1016/j.dsr2.2008.01.006

1. Introduction

Mesoscale eddies are generally thought to play important roles in ocean circulation, heat and mass transport, mixing, biological productivity, upper ocean ecology, fisheries, and biogeochemistry including elemental cycling and fluxes (e.g., Cheney and Richardson, 1976; Olson, 1980; Lobel and Robinson, 1986; Falkowski et al., 1991; Dickey et al., 1993; Allen et al., 1996; McGillicuddy and Robinson, 1997; McGillicuddy et al., 1998; Oschlies and Garcon, 1998; Honjo et al., 1999; McNeil et al., 1999; Letelier et al., 2000; Fischer et al., 2002; Garcon et al., 2001; Leonard et al., 2001; Oschlies, 2001; Seki et al., 2001, 2002; Flierl and McGillicuddy, 2002; Lewis, 2007; Bidigare et al., 2003; Taupier-Letage et al., 2003; Sakamoto et al., 2004). The horizontal dimensions of mid-latitude mesoscale eddy features generally range from about 100 to 250 km in diameter with scaling roughly dictated by the Rossby radius of deformation (e.g., Richman et al., 1977). Fully developed eddies are often in near geostrophic balance although the ageostrophic component can be important. A variety of physical processes have been hypothesized to contribute to mesoscale eddy formation. For example, eddies or rings in the vicinity of western boundary currents like the Gulf Stream and the Kuroshio may be generated through inertial instabilities, open ocean eddies may be produced through baroclinic instabilities, and eddies formed in the vicinity of sea mounts may be caused by barotropic instabilities.

Islands can clearly perturb ocean circulation patterns as well documented for the Hawaiian Island chain (e.g., Qiu et al., 1997; Lumpkin, 1998). Further, mesoscale eddies are also often evident near islands as indicated by the observations reported here and elsewhere (Patzert, 1969; Barton, 2001; Lumpkin, 1998). It has been suggested that instabilities associated with current flow past islands or through island passages can generate eddies (Aristegui et al., 1994, 1997; Barton et al., 2000). Another mechanism for generating eddies involves the acceleration of winds through island channels with high mountains on either side. Gradients in the wind fields on the lee sides of such islands can produce wind-stress-curl distributions that result in localized oceanic upwelling and downwelling and both warm-core and cold-core mesoscale eddies. The latter mechanism appears to explain the production of eddies in the lee of the Hawaiian Islands based on the results of previous investigators and our current study (Patzert, 1969; Lumpkin, 1998; Holland and Mitchum, 2001; Chavanne et al., 2002). It is worth emphasizing that warm-core anti-cyclonic eddies are also produced via the wind-stress-curl mechanism as well as by a shear instability mechanism by drawing energy from the North Equatorial Current as it impinges on Hawaii and separates at the southern tip of the island (Lumpkin, 1998). As noted by an anonymous reviewer, these warm-core eddies may interact with adjacent cold-core eddies and act to suppress biological productivity where they originate and propagate. Our focus here is principally on cold-core eddies, which were sampled directly during our studies. Interaction among eddies is considered in other E-Flux papers.

The central goal of the E-Flux experiment was to improve our fundamental understanding of the coupling of physical, biological, and biogeochemical processes that occur within mesoscale eddies. Importantly, some researchers have suggested that mesoscale eddies are major contributors of carbon to the deep sea (McGillicuddy et al., 1998) while others argue that they may have less of an impact than suggested by McGillicuddy et al. (1998) (e.g., Oschlies and Garcon, 1998). This controversy bears directly on establishing the roles and modeling of mesoscale features as they may affect elemental budgets, fluxes, and the ecology of the upper ocean. More specifically, the effects of such features on nutrient availability, primary production, biological community structures and size distributions, and fluxes of elements including carbon and silicon to the deep sea remain contentious.

The recurrent nature of eddies to the west of the Hawaiian Islands during persistent trade wind conditions was a primary stimulus for the present E-Flux experiment. In particular, it has been previously reported that westward propagating cyclonic eddies are produced in the lee of the Hawaiian Islands on time scales of 50–70 days (Lumpkin, 1998; Seki et al., 2002). Previous studies in the lee of the Hawaiian Islands and North Pacific environs have demonstrated that cold-core mesoscale eddies play significant roles in the region's biogeochemistry, biology, and fisheries (Lobel and Robinson, 1986; Falkowski et al., 1991; Leonard et al., 2001; Seki et al., 2001, 2002; Bidigare et al., 2003; Vaillancourt et al., 2003). Thus, E-Flux investigators conducted a series of three dedicated field experiments to address the various biogeochemical mechanisms hypothesized to lead to enhanced carbon export. This paper reviews the general background of each of the three separate field experiments, the sampling strategies and methods employed, and general observational results with emphases on physical and bio-optical aspects.

2. Observational site, objectives, and methods

2.1. Site

Although mesoscale eddies are rather ubiquitous in the ocean, they remain difficult to study in sufficient detail because they are generally ephemeral and evolve too quickly in geographically diverse locations to be easily sampled using present-day observational tools (Bidigare et al., 2003; Dickey and Bidigare, 2005). With these constraints in mind, the site for the E-Flux field experiments, to the west of the southeastern Hawaiian Islands of Maui and Hawai'i, was chosen on the basis of several criteria. First, it was deemed important to choose a region where mesoscale eddies regularly form. Historical hydrographic and satellite data sets (Patzert, 1969; Lumpkin,

1998; Chavanne et al., 2002; Seki et al., 2001, 2002; Bidigare et al., 2003) indicated that mesoscale eddies typically develop and persist for weeks to several months to the west of the Hawaiian Island chain during persistent trade wind conditions (winds generally from the northeast). In addition, previous studies in this portion of the ocean have indicated that regional cyclonic eddies have significant biological and biogeochemical signatures (Seki et al., 2001, 2002; Bidigare et al., 2003; Vaillancourt et al., 2003). From a practical standpoint, it was also desirable to conduct our field experiments in a region that was readily accessible from a major port to minimize ship transit times and thus to maximize ship sampling capabilities. Moreover, the observations needed to be conducted in deep oceanic waters that were relatively uninfluenced by coastal processes (i.e., coastal upwelling, jets, and filaments as well as rain runoff) so that the results would have general applicability to open ocean settings. All of these criteria were met by the region to the west of the islands of Maui and Hawai'i. The three E-Flux field experiments, which lasted approximately three weeks each, spanned the period of November 4, 2004 to March 28, 2005; specifically, E-Flux I November 4–22, 2004; E-Flux II January 10–28, 2005; and E-Flux III March 10–28, 2005. The periods selected for the experiment were based on wind climatology, essentially optimizing the chances for strong and persistent trade winds. It is worth noting that a multi-platform approach was used to optimally sample mesoscale features with the best possible temporal and spatial resolution under the budgetary and logistical constraints of the project. Thus, satellites, ships, and drifters were utilized in the collection of our data sets.

2.2. Observational objective and methods

The primary observational objective for the three E-Flux field experiments was to obtain interdisciplinary data to enable the location, characterization, and interpretation of the physical, optical, biogeochemical, and biological structures and dynamics of mesoscale eddy features off Maui and Hawai'i. The R/V *Ka'imikai-O-Kanaloa* (*KOK*) was used for the E-Flux I experiment and the R/V *Wecoma* was used for the E-Flux II and III cruises. The methods used for the physical, bio-optical, and chemical measurements during the three E-Flux field experiments were quite similar although some instrumentation differed between the two research vessels. For convenience, the general methodologies used for the three experiments are presented within the following subgroups: (1) ship-based profile measurements, (2) ship-based acoustic Doppler current profile (ADCP) measurements, (3) drifter measurements, (4) satellite measurements, and (5) an overview of measurements.

(1) *Ship-based profile measurements*: During the E-Flux cruises, measurements were made with profiled CTD/rosette packages at stations deemed to be very near the centers of mesoscale eddy features (called IN stations), along several intersecting horizontal transects that were selected to pass through the best-estimated centers of the eddies, and well outside of them (called OUT stations). The CTD systems were used to measure temperature, conductivity, pressure, chlorophyll *a* fluorescence, beam transmission (660-nm) or light backscattering (for inferring particle concentrations and distributions), photosynthetic available radiation/scalar irradiance (PAR), and dissolved oxygen. Details concerning specific sensors may be found on University of Hawai'i SOEST (R/V *KOK*) and Oregon State University (R/V *Wecoma*) websites (http://www.soest.hawaii.edu/HURL/KOK_specs.html, http://www.shipsops.oregonstate.edu/ops/wecoma/). During E-Flux I, a 24-bottle, 12-L rosette was used to collect water samples, whereas a 12-bottle rosette sampler equipped with 10-L bottles was used for E-Flux II and III operations. Multiple profiles were generally made to depths of approximately 500, 1000, or 3000 m. Rosette bottles were tripped at multiple depths, which were selected on the basis of the vertical structure of the physical, optical, chemical, and biological variables (i.e., in the mixed layer, at the depth of a selected isopycnal surface, within the euphotic zone, and in the deep chlorophyll maximum region). The CTD sensors were calibrated after each cruises (bottle samples were not used for salinity calibration). The sampling rate of the CTDs (SBE 9/11 + units) was 24 Hz, and most profiles were done with a vertical profiling rate of $0.50\,m\,s^{-1}$. Data were recorded during both up- and downcasts. The SBE Data Processing software suite was used to convert the raw binary data into engineering units. Manufacturer's configuration files were used in the process. The same software was used to further process the data following the procedures described in the SBE Data Processing User Manual (http://www.seabird.com/pdf_documents/manuals/SBEDataProcessing_7.10.pdf).

A low-pass filter (default time constant of 0.15 s) was applied to the pressure record in order to smooth out high frequency data (see Sea-Bird SBE Data Processing User Manual for details). An alignment procedure also was applied to account for the different positions of the sensors on the rosette and their respective response times. CTD data collected during excessive ship roll were eliminated, thus removing the bins recorded when the vertical profile velocity was less than $0.15\,m\,s^{-1}$. Data were then averaged into 1-m (1-db) bins and salinity and density were derived from temperature, conductivity, and pressure measurements following the UNESCO equations (UNESCO, 1981). More information concerning the CTD data processing procedure can be found on the Sea-Bird website given above and an OPL Data Report (http://orca.opl.ucsb.edu:8080/plone/eflux/eflux3/casts/Data_Processing_v1.3.pdf). After processing, the CTD data also were quality controlled by

comparing CTD values with climatological data for the experimental region. Data values that were different by more than two standard deviations (i.e., outliers) from the climatological mean were eliminated.

Samples for nitrate + nitrite ($\mu M\ L^{-1}$) and chlorophyll *a* ($mg\ m^{-3}$) were collected at discrete depths using the rosette sampler (see Rii et al., 2008). Nitrate + nitrite samples were analyzed in the laboratory using a Technicon Autoanalyzer II. For determinations of chlorophyll *a*, 2-L water samples were filtered immediately after collection and analyzed (post-cruise) using high performance liquid chromatography. These discrete values of total chlorophyll concentration were used to determine the total chlorophyll–fluorescence regression coefficients for the E-Flux I and III cruises. These coefficients were then used to convert fluorescence voltage into total chlorophyll *a* concentrations. Unfortunately, for the E-Flux II cruise it was not possible to compute the regression coefficients, because HPLC measurements on the collected water samples were not available; therefore the conversion was made using the same coefficients computed for the E-Flux III cruise (same fluorometer). The 1% light level depths were directly computed from scalar irradiance (PAR) profiles for the CTD casts collected during daytime. These data were used to compute the relationship between the 1% light level depths and the mean total chlorophyll concentrations between the surface and the 1% light level depths. The coefficients were then used to derive the 1% light levels depths for the casts collected at night from total chlorophyll *a* concentration data (Morel, 1988). Unfortunately, no discrete dissolved oxygen data were obtained from the water samples, and thus it was not possible to properly post-calibrate the dissolved oxygen sensor. Hence, it is not possible to verify the accuracy of oxygen concentrations. Nonetheless, individual profiles can still be compared within a specific cruise, but it is not possible to compare absolute oxygen concentration values between cruises.

For some profile measurements, a specialized optics package was tethered 1.5 m beneath the CTD/rosette. The optics package was equipped with two spectral absorption–attenuation instruments (WETLabs AC-9 and AC-S), a fluorometer/turbidity instrument (WETLabs FLNTU), and a Sea-Bird CTD. Also, both ships collected meteorological and near-surface (flow-through) physical, chemical, and biological data. Neither the optics package data nor the ship underway data are discussed in the present report.

(2) *Ship-based ADCP data*: The simultaneous mapping of upper ocean currents as functions of depth and geographic position was a critical part of the E-Flux experiment. ADCP data were used not only to determine the dimensions of the eddies, but also to locate the positions of the eddy centers and to choose the transect paths that intersected them.

Profiling ADCPs (VM150 kHz Narrow Band manufactured by RDI) were provided by the R/V *KOK* and R/V *Wecoma*. The current data were recorded as 15-min averages in 10-m bins from 40 to 450 m depth. The data acquisition systems were linked to GPS and heading systems to provide accurate position data as well. Details concerning the ADCP instrumentation and data processing routines may be found on the R/V *KOK* and R/V *Wecoma* websites.

(3) *Drifters*: Drifters were deployed during each of the E-Flux experiments. In particular, a surface drifter (called OPL Drifter) with a 1.5-m cylindrical foam core and 1-m cross-shaped drogue (located at depths of either 80 or 90 m) was deployed to track the fluid motion of the eddies. In addition, the OPL drifter was used to obtain a nearly Lagrangian time series (1-min sampling intervals) of temperature from near the surface to a depth of 150 m at 10-m intervals using internally recording temperature sensors (Onset Inc.). Geographic coordinates of the drifter were obtained through the Argos communication satellite system and these data were transmitted to the Ocean Physics Laboratory (OPL) in Santa Barbara. The position data were then forwarded to scientists onboard the research vessels via email for near real-time tracking of the drifter. Temperature data were offloaded after recovery of the drifter and time series were plotted. This drifter was recovered once, but was lost later in the experiment.

A bio-optical surface drifter (METOCEAN), which was not drogued, was deployed during the E-Flux I and III cruises. The surface drifter provided temporal measurements (data were acquired every 3 h) of drifter position, barometric pressure, air temperature, sea-surface temperature (SST), and chlorophyll *a* concentration. These data were transmitted via satellite to OPL in Santa Barbara and then emailed back to the research vessel for examination and plotting of positions. The chlorophyll *a* concentrations were found to be in generally good agreement with those obtained from the ship measurements.

Finally, a drifting sediment trap array (Rii et al., 2008), though not designed as a Lagrangian drifter, was also useful for tracking the general patterns of motion of the eddies. The trap array, which represented the major current drag element, consisted of 12 particle interceptor traps (PITS) suspended at a depth of 150 m. The location of the array was obtained through an Argos satellite transmitter; geographic coordinates were then sent via email to the ship. For recovery purposes, the array was also equipped with an RDF radio and strobe lights. Samples obtained from the traps were used by other E-Flux investigators to examine the influence of eddy pumping on the export rates of particulate carbon, nitrogen, phosphorus, biogenic silica, and taxon-specific pigments.

(4) *Satellite measurements*: Satellite-based sensors provide generally synoptic views of the ocean surface on scales relevant to mesoscale eddies. Satellite sensors that were useful for the E-Flux field experiments included NASA's QuikScat scatterometer for surface winds, NOAA's Geostationary Operational Environmental Satellites (GOES) for SST, and NASA's MODIS for SST and ocean color (surface chlorophyll). Satellite altimetry data were inspected, but were generally found to have insufficient spatial (between tracks) resolution to provide useful quantitative information for our study region and moreover for oceanic mesoscale processes (Alsdorf et al., 2007). However, it is worth noting that a composite image (TOPEX/JASON/ERS) obtained during E-Flux III does appear to show Cyclone *Opal* and warm anti-cyclonic features to the northwest and south of *Opal* (see Nencioli et al., 2008). QuikScat, which is a polar orbiting satellite, provided wind data over a 1800 km wide swath for our study region (see QuikScat website: http://podaac-www.jpl.nasa.gov/cgi-bin/dcatalog/fam_summary.pl?ovw+qscat). The retrievals of wind speed and direction from QuikScat gave twice-daily data with spatial resolution of 25 km × 25 km on the earth's surface.

NOAA's OceanWatch Central Pacific program (see website: http://oceanwatch.pifsc.noaa.gov/) provided SST products derived from NOAA's GOES. These products were created by combining three separate images with 6-m pixel resolution, each created 1 h apart and retaining the most recent temperature value. Therefore, near real-time NOAA SST image products were updated every 3 h. Because of the variable and often persistent cloud cover near the Hawaiian Islands, these 3-h products were then collated by the Central Pacific Ocean Watch to provide a 24-h SST composite image that was updated daily. NASA's MODIS SST product was created with 4.6-km pixel resolution with daily and eight-day composites. For tracking the eddy formation and decline, the daily products were used. The MODIS Aqua satellite images the full earth every 1–2 days, therefore the daily composites usually provided coverage over our study area every other day. The NASA Ocean Color group provided binned, daily mapped, and eight-day composite surface chlorophyll *a* imagery derived from MODIS Aqua optical imagery. This imagery had 4.6-km ground pixel resolution with chlorophyll *a* concentration being calculated using the standard NASA data processing routines and algorithms (see http://oceancolor.gsfc.nasa.gov/PRODUCTS/; Campbell et al., 1995).

The collective satellite-derived data products were used for identifying periods when trade winds occurred and persisted, approximating when mesoscale eddies formed and dissipated, and estimating the scales of the surface manifestations of the eddy features. These data also enabled the optimal initiation of ship-based sampling, placement of drifters in the proximal centers of eddies, and tracking of the movements of the eddies during the field experiments. It should be noted that satellite-derived chlorophyll *a* and SST imagery were often unobtainable due to cloud cover. In addition, only near-surface expressions of the eddies' physical and biological effects could be monitored and subsurface features could not be discerned. Thus, our satellite-based determinations of initiation and cessation times of mesoscale eddies are only estimates with likely uncertainties of roughly 1–2 weeks.

(5) *Measurement overview*: The multi-platform sampling approach used for the E-Flux study was essential and enabled the collection of interdisciplinary data spanning multiple time and space scales as synoptically as possible under the experimental constraints (Dickey and Bidigare, 2005). One of the greatest in situ sampling challenges for E-Flux was to locate the centers of the mesoscale eddies. The three primary methods follow:

- GOES satellite SST images (and MODIS chlorophyll *a* when available) were inspected and the coordinates of the geometrical center of each eddy were estimated. These images along with the MODIS SST images were also useful for estimating the lifetime of each eddy since ship time and thus experiment duration were necessarily limited. However, it is important to emphasize that the satellite-derived lifetimes of the eddies were probably underestimates as they likely existed before and after their appearances in SST and color imagery. Also, cold-core mesoscale eddies can be capped by relatively warm waters and thus hidden or even appear as warm-core eddies. A dramatic example of this latter situation is described by Seki et al. (2002), who suggest that the cyclonic eddy of their study moved into the wind shadow of Hawai'i where diurnal heating acted to form a very near-surface warm-water cap over the cold-core eddy. It also should be noted that the surficial manifestations of horizontal scales of the eddies were smaller than their subsurface signatures (by at least a factor of 2 or more in scale).
- Ship-based real-time underway surface sampling systems measured several variables including temperature (and chlorophyll *a*) from water flowing through the ship's intake system. The continuously ship-sampled SST values along transects were used to determine if the research ships were near the centers of the cyclones.
- The ships' near real-time ADCP horizontal current recording systems were used for several purposes. The transect data (usually 40-m depth record) were inspected and the centers of the cyclones were deemed to be located where the ADCP-determined currents were minimal or near zero (see Nencioli et al., 2008, for details). Useful information was also retrieved from the directions of the current vectors, as they reversed direction after passing through the

cyclones' centers, as well as from the angles of the velocity vectors with respect to the ship's track (radial tracks being characterized by velocity vectors perpendicular to the track). In some cases, inferences of eddy centers were possible only after having performed multiple transects near the actual centers.

The ADCP method generally proved to be the most reliable technique for finding the cyclone centers, particularly when used in conjunction with the ships' underway SST and CTD records. ADCP data were not displayed in real-time during E-Flux I, so the CTD and optics package profile data were vital; however, ADCP data were displayed in real-time for E-Flux II and III. The ADCP data were used to produce near real-time vector maps using the Matlab m_map suite. These maps were used to track the positions of the centers of the eddies. Contours of other key variables collected during transects, which included horizontal currents, temperature, salinity, density (or sigma-t, σ_t), and chlorophyll a fluorescence, were also created in near real-time using Surfer software. These plots were used to determine the cyclones' spatial extents as well as to estimate distributions of chlorophyll a (i.e. the chlorophyll a maximum layer), mixed layer depth, key isopycnal surfaces, property maxima and gradients, and maximum velocity and shear zones.

During the experiments, drifters were deployed near the estimated centers of the eddy features. Following the experiments, drifter tracks were analyzed. By examining the drifter trajectories (i.e. using the geometric center of the roughly circular trajectories), useful complementary information concerning the movement of each eddy was derived.

3. Results

3.1. Overview

Some of the principal results of each of the three E-Flux field studies are presented next. First, it is worth re-emphasizing that the cold-core mesoscale eddies appearing to the west of Hawai'i are quite likely correlated with strong and persistent northeasterly trade winds that blow through the 'Alenuihaha Channel that separates the islands of Maui and Hawai'i. The trade wind air-flow between these islands is accelerated because of the presence of mountains, Haleakala on Maui and Mauna Kea on Hawai'i, as discussed by Patzert (1969) and Chavanne et al. (2002). Fig. 1 shows a time series of wind velocity

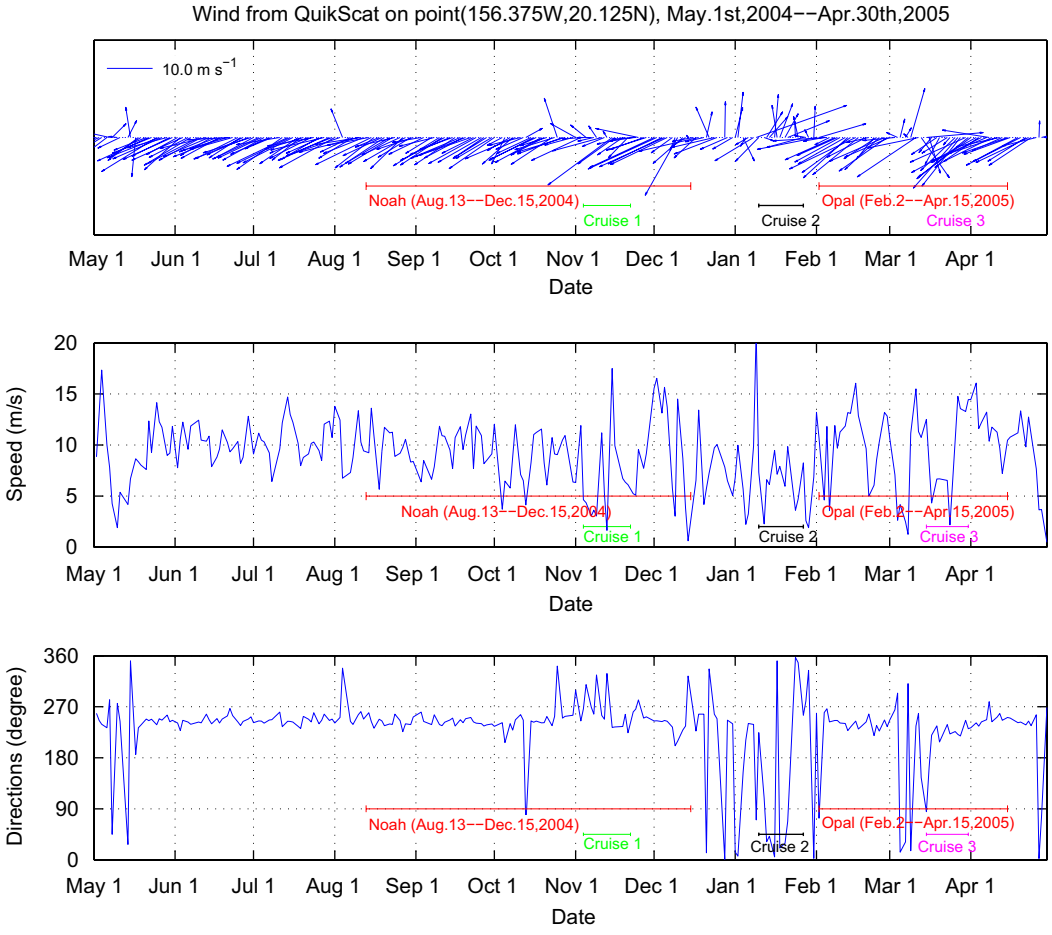

Fig. 1. Time series of winds preceding, during, and shortly after the E-Flux experiment outside the 'Alenuihaha Channel at 20.1°N, 156.4°W (top: wind stress vectors; middle: wind speed; bottom: wind direction).

vectors, wind speed, and wind direction obtained from a site to the southwest of the 'Alenuihaha Channel (20.10°N, 156.40°W; noted with a blue triangle in Figs. 2, 7, and 11). The location chosen for the display of wind time series is in the general area where cold-core mesoscale eddies or cyclones spin up as typified by the initial appearances of previous eddies and those observed during E-Flux I and III (Figs. 2B and C and 11B and C). Relatively strong and persistent trade winds (northeasterly) occurred from late May 2004 through late April 2005 with only a few exceptions (Fig. 1). The most notable exception occurred from early December 2004 through early February 2005, a period during which the E-Flux II cruise took place and no mesoscale eddies were observed despite intensive sampling. Interestingly, cold-core eddies were evident in satellite SST data downwind of the 'Alenuihaha Channel or to the west of Hawai'i during persistent trade wind conditions during the periods of July 2004 (an unnamed cyclone occurred prior to the first E-Flux cruise; this feature drifted off to the west before Cyclone *Noah* formed), mid-August through mid-December, 2004 (Cyclone *Noah* was observed during the E-Flux I cruise), and early February through mid-April, 2005 (Cyclone *Opal* was observed during the E-Flux III cruise). These observations support the hypothesis that persistent trade winds are the likely forcing mechanism responsible for producing cold-core cyclones off Hawai'i.

The following descriptive narratives proceed chronologically and utilize satellite, ship-based, and drifter data sets. More comprehensive and detailed analyses of the E-Flux physical, bio-optical, and chemical data sets are discussed in other papers in this volume (see Kuwahara et al., 2008, for E-Flux I, and Nencioli et al., 2008, for E-Flux III). E-Flux III results are also highlighted in Benitez-Nelson et al. (2007).

3.2. E-Flux I

The primary focus of the E-Flux I cruise (November 4–22, 2004, YD 309–327) was a cold-core mesoscale eddy, Cyclone *Noah*. Cyclone *Noah* first appeared in MODIS and GOES SST satellite imagery between August 13 and 20, 2004 with its center located at ~20.20°N, 156.40°W. The feature appears to have spun up to the southwest of the 'Alenuihaha Channel as a result of strong and persistent northeasterly trade winds between the mountains of Haleakala and Mauna Kea through the 'Alenuihaha Channel (Fig. 1). Noah drifted slowly southward for a brief time after formation, but then remained near 19.60°N, 156.50°W for most of the E-Flux I cruise sampling period. Lower wind speeds are evident downwind or in the lees of the islands before and during E-Flux I (Figs. 2A–C). During this same time period, warm-water wakes are evident downwind of the islands of Oahu, Maui, and Hawai'i, while cooler waters lie downwind of the channels separating these islands (Figs. 2B and C). It is quite possible that the genesis of *Noah* occurred in early August 2004, since SST and ocean-color sensors only measure the surface expressions of mesoscale eddies and clouds often obscure the surface in our study region. Nonetheless, these SST satellite data were extremely valuable in that they allowed us to target the approximate center of Cyclone *Noah*, initiate ship survey (transect) observations using our CTD/rosette profiler and underway ADCP, and eventually to launch drifters in the central portion of the eddy.

Satellite SST and ocean-color images were emailed to the R/V *KOK* to help guide the ship-based and drifter in situ sampling program. Based upon SST images of November 5–6, 2004, a series of four CTD/optics package transects were made in order to map the cold-core Cyclone *Noah* (Fig. 3). Table 1 presents the locations and start and end times for each of the transects. Transect 3, the so-called "money run" transect, was the most intensively sampled of all transects. This particular transect is used to highlight specific biogeochemical and biological features of this eddy. The initially targeted center of the eddy was assumed to lie along latitude 19.50°N. The eddy mapping area covered a rectangular area from approximately 18.83 to 20.33°N and 156.02 to 157.17°W. The sampling area covers approximately $20,000\,km^2$, which is much larger than the area of the island of Hawai'i ($10,458\,km^2$). The sequence of eddy mapping stations is indicated by the numbers in Fig. 3 and spanned the period of 1400 November 6 through 0930 November 11 (local times) or slightly more than six days (Table 1). Station intervals of roughly 17 km (~10 nmi) were used for the transects as indicated in Fig. 3.

The first transect (Transect 1) ran from west to east and ship-based temperature and density data were contoured in horizontal dimension and depth using contouring routines. It was determined that the best estimate of the longitude of the center of the eddy was located along 156.52°W based upon the central location of the doming of the isotherms and isopycnal surfaces (i.e., the minimum depth of the σ–$t = 23.0\,kgm^{-3}$ isopycnal reference surface or σ–t_{23} contour, which lay near the top of the thermocline, was especially useful for this purpose). The second transect (Transect 2) was perpendicular to the first. Again, contouring of the temperature and density data was used to better define the location of the center of the eddy in analogy to the procedure used for the east–west line. The best estimate of the center of the eddy was then determined to be at Station 13 or 19.67°N, 156.52°W, which is likely within a few km of the true geometric center of the eddy feature. This station was subsequently used for more intensive sampling (called the IN Station).

Transects 3 and 4, running at 45° with respect to the east–west and north–south transects, were then conducted (Fig. 3). The patterns ran from the northwest to the southeast and then from the northeast to the southwest. The star sampling pattern was then completed and data were contoured as transect sections with respect to depth and in plan view on depth and density horizons. Based on the four transects, it was concluded that the new sampling center was within a few km of the true geometric center of the eddy. It was anticipated that Cyclone *Noah* might move

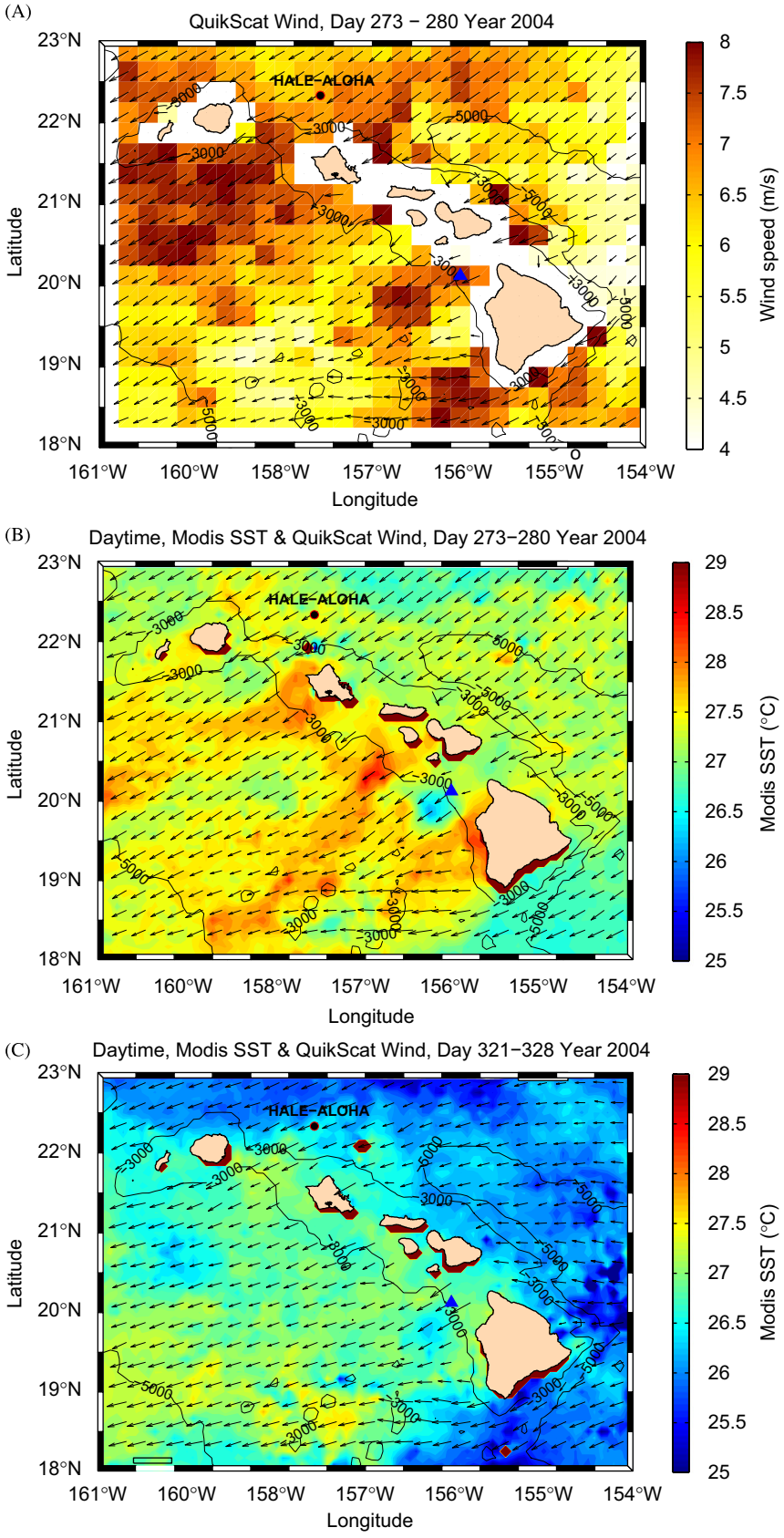

Fig. 2. QuikScat wind vectors with wind speed magnitude shown in color prior to E-Flux I (September 29–October 6, 2004; YD 273–280) (A). MODIS sea-surface temperature in color and QuikScat wind vectors prior to E-Flux I (September 29–October 6, 2004; YD 273–280) (B), and during E-Flux I (November 16–23, 2004; YD 321–328) (C). Blue triangles indicate location of time series of winds shown in Fig. 1.

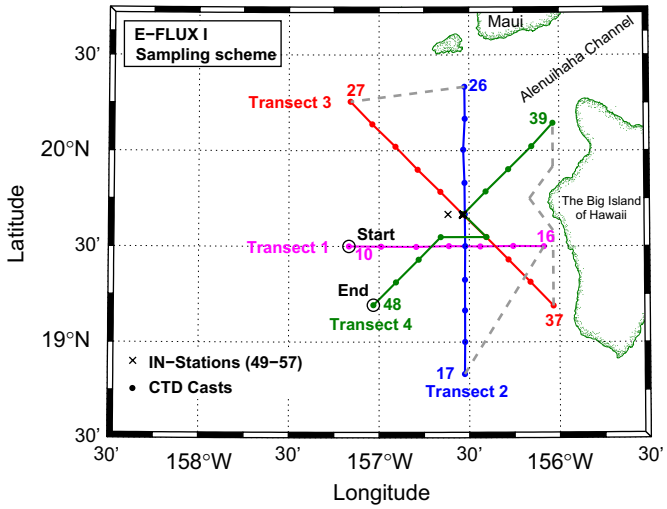

Fig. 3. Sampling map for E-Flux I. X indicates the location of IN-Station CTD casts.

Table 1
Dates and times (Hawaii Standard Time, local time) of the beginning and end of R/V *KOK* sampling operations during transects (see Fig. 3) and time series stations inside ("IN Stations") and outside ("OUT Stations") of E-Flux I

Operation	Beginning date (2004)	Beginning time (HST)	Ending date (2004)	Ending time (HST)
Transect 1	Nov. 6	1400	Nov. 7	0353
Transect 2	Nov. 7	1206	Nov. 8	1301
Transect 3*	Nov. 8	2004	Nov. 9	0140
Transect 4	Nov. 9	0140	Nov. 11	0930
IN Stations	Nov. 11	1400	Nov. 17	1800
OUT Stations	Nov. 4	2330	Nov. 6	0400
OUT Stations	Nov. 18	1700	Nov. 20	1300

*Indicates the so-called "money run" transect which was the most intensively (more variables) sampled transect of the cruise.

during the six days of our ship-based transect sampling. However, data collected during a subsequent visit to the final sampling center and available satellite images indicated that the eddy center had not moved by more than a few km, a distance that is likely within the uncertainty of our estimated eddy center.

Although the initial surface expression (e.g., from satellite SST imagery) of Cyclone *Noah* was limited in horizontal scale to only about 40 km, analysis of ship transect-depth profiles (Fig. 4) revealed a fully developed elliptical cyclonic feature (with its major axis being oriented northwest to southeast with a length of about 130–150 km based on the distance from the center of the eddy at which the σ–t_{23} isopycnal surface was nearly level) as evidenced by its size, its tangential speeds (~40–60 cm s^{-1}; Fig. 5), and outcropping of several physical and biological properties (Fig. 4). More specifically, the 24.5 °C isotherm rose from about 125 m outside the eddy to about 65 m near the eddy's center, the 35 psu isohaline surface rose from about 125 m

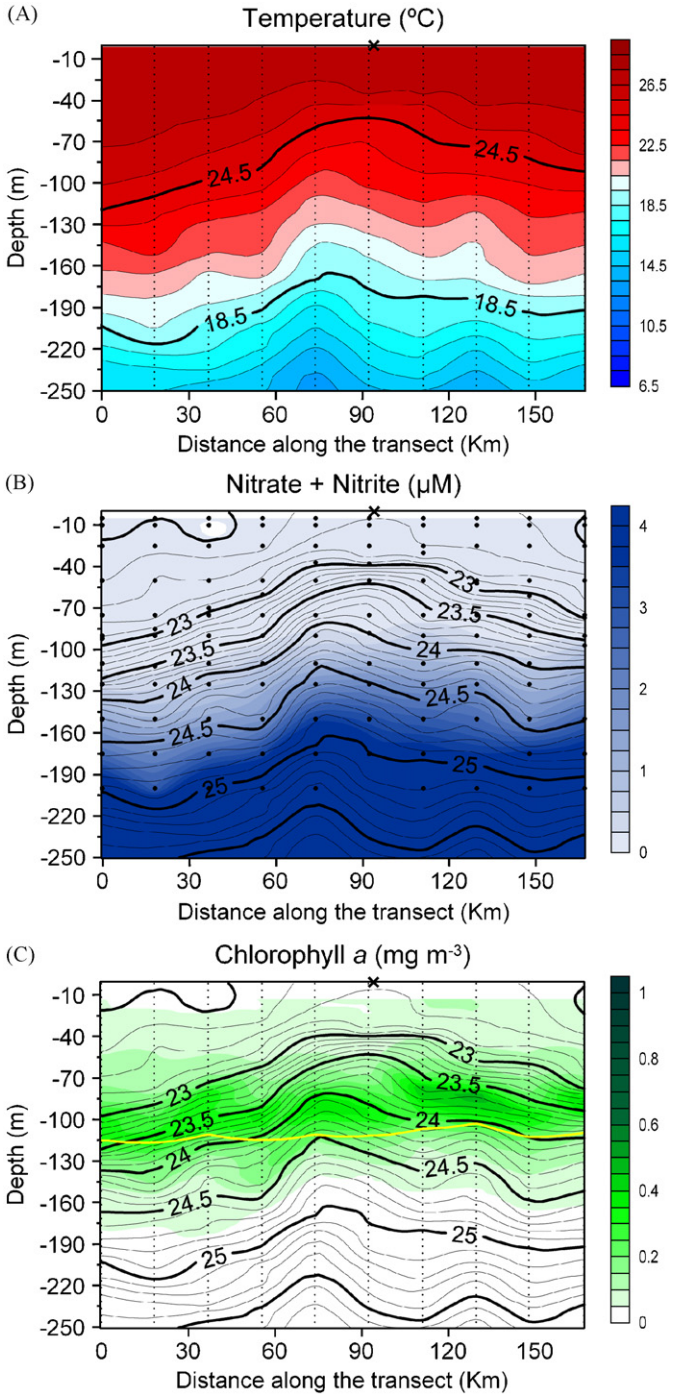

Fig. 4. Transect data for Transect 3 during E-Flux I. (A) Temperature (°C). (B) Nitrate + nitrite in color (μM). Isopycnal surfaces are shown with units of kg m^{-3}. (C) Chlorophyll *a* in color (mg m^{-3}). Isopycnal surfaces are shown with units of kg m^{-3}. Depth of the 1% light level is shown in yellow curve. The black X at 0 m depth indicates the position along the transect closest to the best-estimated location of the center of *Noah*.

outside the eddy to about 50 m near the eddy's center (not shown, see Kuwahara et al., 2008), and the 23.8 σ–t isopycnal surface rose from about 125 m outside to about 75 m at the eddy's center (not shown). Outcropping of isopycnals is also evident within a rough distance of 10–30 km of the eddy's center.

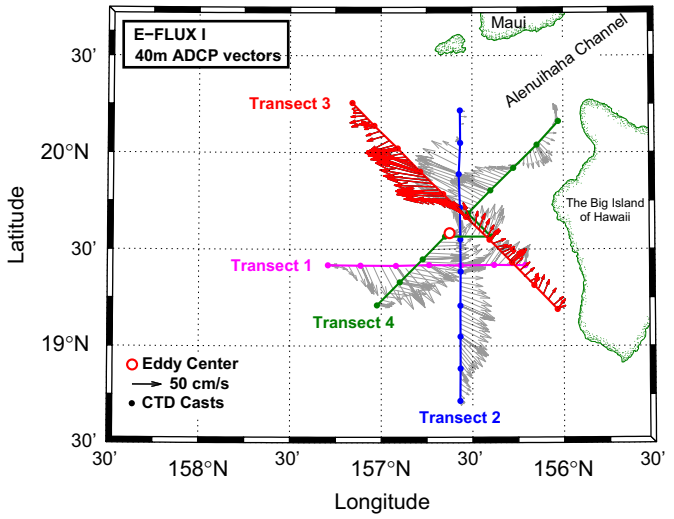

Fig. 5. ADCP current vectors in the upper layer (40 m) during E-Flux I. For every transect the position of the center of the eddy has been determined. The transects have been positioned with respect to the center of Transect 3.

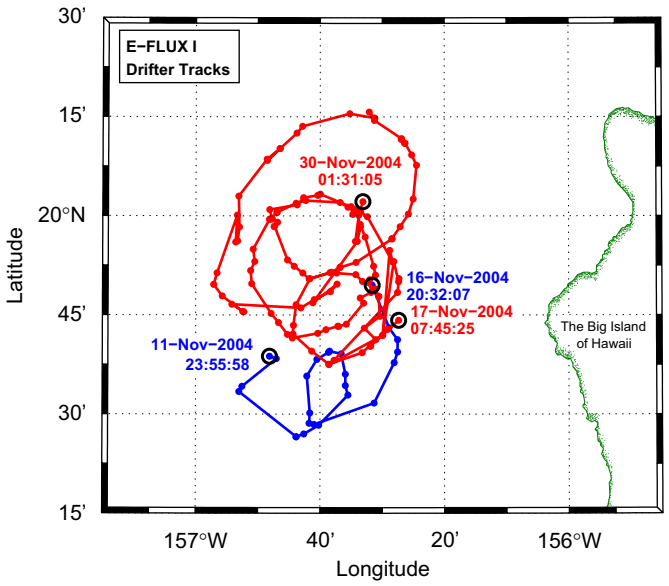

Fig. 6. Drifter trajectories during E-Flux I.

A subsurface inner-core of high-salinity water was centered at a depth of about 80 m in the region of the eddy's center (note: salinity data are displayed in Kuwahara et al., 2008). A central chlorophyll *a* maximum peak (concentrations greater than 0.5 mg m^{-3}) was located at a depth of roughly 75–80 m and its horizontal position was virtually co-located with the geometric center of the eddy. The chlorophyll *a* maximum layer deepened away from the center of the eddy and chlorophyll *a* concentration decreased radially. The chlorophyll *a* maximum layer was loosely bounded by isopycnal surfaces of 24–23.5 kg m^{-3}, and there was a good correspondence between chlorophyll *a* and particulate maxima (not shown here). The inner-core region of slightly higher chlorophyll *a* was apparently less than 15 km in diameter. The 1% light level depth is also indicated in the chlorophyll *a* panel of Fig. 4. The uplifting of nutrients into the euphotic layer and the increased chlorophyll *a* levels toward the center of the eddy are consistent with enhanced nutrient stimulated productivity within cold-core eddies. The overall extent of the eddy shows strong anomalies reflected in lower temperature, higher salinity, greater density, higher nitrate + nitrite concentrations, and higher chlorophyll *a* concentrations (Kuwahara et al., 2008; Rii et al., 2008).

Horizontal currents at 40-m depth are displayed in Fig. 5 to provide an overview of the current structure of Cyclone *Noah*. The current magnitudes increase roughly linearly as a function of distance from the eddy center before starting to decrease at distances of roughly 40–60 km from the eddy center. Maximum tangential current velocities reached about 60 cm s^{-1}. Drifter trajectories obtained within *Noah* are displayed in Fig. 6 and clearly show the cyclonic motion of the feature and suggest its ellipticity. It appears that the OPL surface drifter made two revolutions around the eddy's center. These data were useful in estimating the eddy center and approximate tangential velocities. A METOCEAN bio-optical drifter and a drifting sediment trap array both followed trajectories that were consistent with that of the OPL surface drifter. Previous research on Hawaiian lee eddies by Lumpkin (1998) has indicated that statistically, cyclonic eddies typically translate westward at near the wave speed of a first baroclinic Rossby wave and generally to drift toward the north tending to cause separation from southward drifting anti-cyclonic eddies. Theoretical considerations invoking the β-effect also support westward eddy movement (Cushman-Roisin et al., 1990; Chassignet and Cushman-Roisin, 1991) and eddy–eddy interactions can lead to westward movement as well (Lumpkin, 1998). Interestingly, Cyclone *Noah* did not appear to translate over a significant distance after its formation nor during or after our experiment based on satellite SST and ship-based measurements.

Elliptically shaped eddies, such as Cyclone *Noah*, have been noted in other historical data sets collected in the region (Patzert, 1969; Lumpkin, 1998; Seki et al., 2001, 2002; Bidigare et al., 2003). Complementary ADCP and drifter data (Figs. 5 and 6) and additional remote sensing SST images are not as definitive, but are supportive of this assertion. A clear doming of the σ–t_{23} contour in the eddy's center, which is congruent with enhanced chlorophyll *a* concentrations, implies that Cyclone *Noah*, although likely in a relaxed or spin-down phase, was productive due to nutrient enrichment from subsurface waters (see nutrient transect section in Fig. 4). Interestingly, however, two days of strong trade winds (over 35 knots causing cessation of CTD operations; see Fig. 1) may have acted to re-energize *Noah* for a brief spell as indicated by possible shoaling of the σ–t_{23} isopycnal surface at *Noah*'s center. Satellite SST imagery during the cruise also indicated that the eddy had relaxed and then re-energized over the study period.

3.3. E-Flux II

The E-Flux II field experiment, conducted from January 10 to 28, 2005 (YD 10–28), followed E-Flux I, which ended on November 22, 2004. The wind time series shown in Fig. 1 indicates generally weak winds with variable directions from late December 2004 through the time period encompassing the E-Flux II cruise period. The key point here is that northeasterly trade winds were especially rare during E-Flux II; at times southwesterly winds prevailed (180° with respect to the northeasterly trade wind direction). QuikScat wind vectors and speeds shown in Fig. 7A are representative for E-Flux II. Thus, wind-forcing conditions were clearly unfavorable for the generation of mesoscale eddies. Furthermore, satellite SST images did not indicate the presence of any eddies with surface expressions in the region from mid-December 2004 until early February 2005 (Fig. 7B). Interestingly, warm waters appeared in satellite SST images (i.e., Fig. 7B) to the southwest of the 'Alenuihaha Channel where cold eddies are often spawned.

With no obvious hints of mesoscale features in the study region prior to the E-Flux II cruise, it was decided to first begin mapping surface currents (ADCP data) and subsurface hydrographic and bio-optical variables along selected sections to attempt to discover any sub-mesoscale and/or mesoscale features that might be present outside the detection limits of remote sensors. Data were plotted in

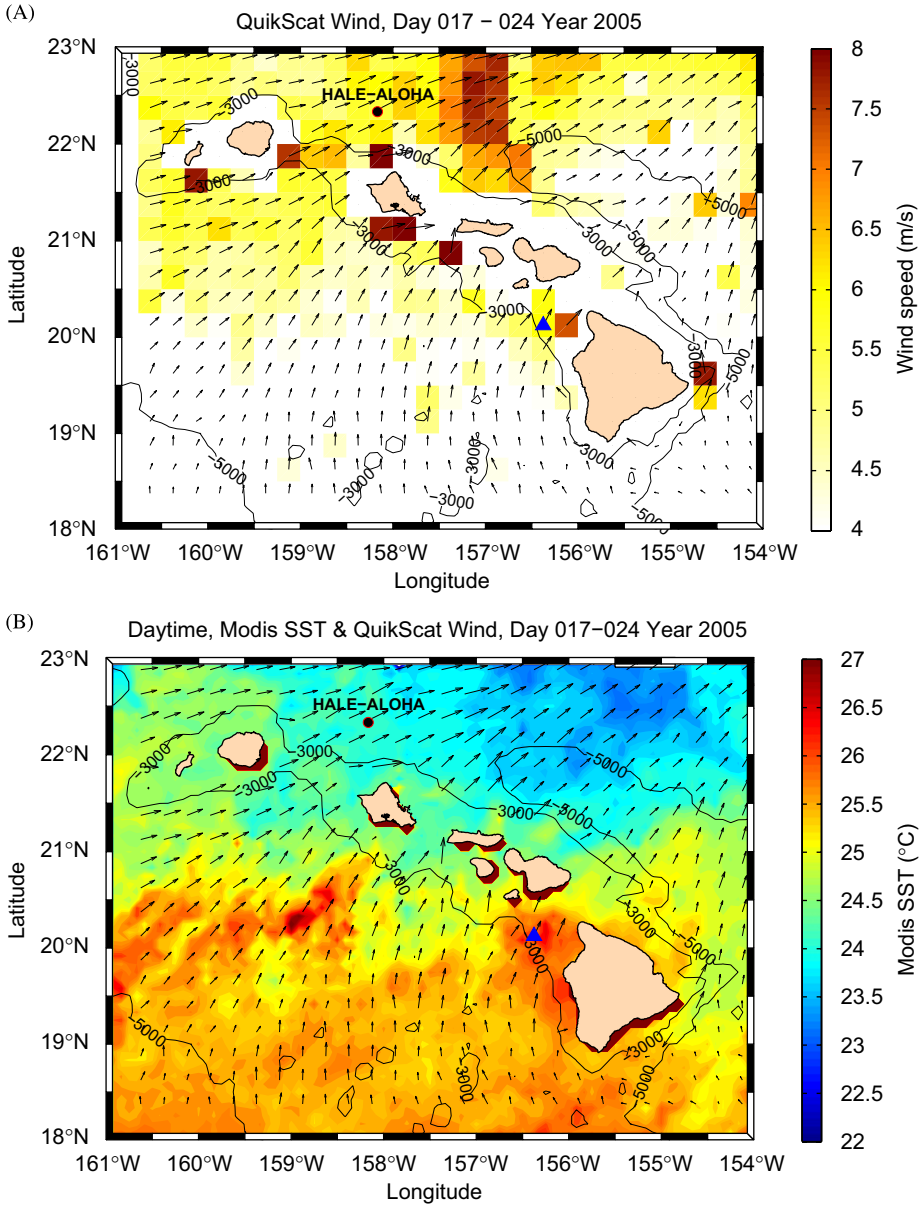

Fig. 7. QuikScat wind vectors with wind speed magnitude shown in color during E-Flux II (January 17–27, 2005; YD 17–27) (A). MODIS sea-surface temperature in color and QuikScat wind vectors during E-Flux II (January 17–24, 2005; YD 17–24) (B). Blue triangle indicates location of time series of winds shown in Fig. 1.

near real-time for inspection. A map indicating the sampling transects for E-Flux II is shown in Fig. 8, and Table 2 presents the start and end times of each of the transects. The first mapping section, Transect 1, was nearly coincident with the transect that passed through the center of the mature eddy (Cyclone *Noah*) studied in detail during E-Flux I. Transect 1 began on January 10 at 20.30°N, 156.50°W and extended southward along 156.50°W to 18.70°N. The spacing between stations was 37 km (~20 nmi) and the time interval between individual CTD casts was about 3 h. No mesoscale features were discovered during Transect 1.

R/V *Wecoma* then began a transect northward (called Transect 2) along longitude 157.00°W (about 55.6-km to the west of Transect 1) from latitudes 18.00°N and 20.30°N, respectively. ADCP data continued to be collected nearly continuously. CTD data were again obtained every 37 km or 20 nmi at 3-h intervals. At this point (January 12), no major mesoscale eddy features were apparent from our data, so Transect 3 was made from the lee side of Maui and Hawai'i (19.30°N, 157.50°W) through the 'Alenuihaha Channel (to 20.70°N, 155.50°W), which separates the two islands. Again, the region lying just to the southwest of the Channel has been documented to be a location where mesoscale eddies are often initiated. Thus, Transect 3 was considered important to determine if sub-mesoscale or mesoscale eddies might be present and also to characterize the physical and bio-optical structures and currents of the 'Alenuihaha Channel and neighboring waters. Transect 3 was selected to be sampled for a multiplicity of biological and biogeochemical variables (i.e. a so-called "money run"). The spacing between CTD stations for this transect was reduced to 18.5 km in order to resolve better any features that might be present. Later transects were made in search of mesoscale or even submesoscale features. Data collected during a second money run, Transect 4, are displayed in Fig. 9. Despite all attempts to discern eddy features from hydrographic and satellite data, no obvious features were evident. ADCP data are shown in Fig. 10. The currents are generally quite weak and no clear indications of mesoscale features are evident. Perhaps the most important result of E-Flux II is the lack of a major mesoscale feature or any major spatial biological or biogeochemical anomalies in the absence of trade wind conditions.

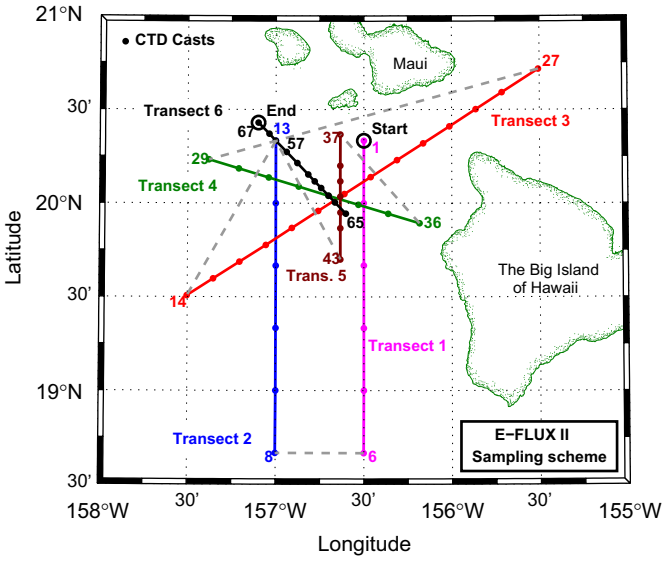

Fig. 8. Sampling map for E-Flux II.

Table 2
Dates and times (Hawaii Standard Time, local time) of the beginning and end of R/V *Wecoma* sampling operations during transects (see Fig. 8) for E-Flux II

Operation	Beginning date (2005)	Beginning time (HST)	Ending date (2005)	Ending time (HST)
Transect 1	Jan. 10	1800	Jan. 11	0900
Transect 2	Jan. 11	1826	Jan. 12	0855
Transect 3*	Jan. 12	1520	Jan. 14	0640
Transect 4	Jan. 14	1800	Jan. 15	0747
Transect 5	Jan. 15	1145	Jan. 15	2026
Transect 6*	Jan. 18	0840	Jan. 19	1815

*Indicates the so-called "money run" transects which were the most intensively (more variables) sampled transects of the cruise.

3.4. E-Flux III

Strong northeasterly trade winds returned to the southwest of the 'Alenuihaha Channel within a week of the completion of the E-Flux II cruise as indicated in Fig. 1 and produced a cold-core, cyclonic eddy called Cyclone *Opal* (Figs. 11A–C). Except for about 10 days in very late February through early March 2005, the trade winds persisted from the beginning of the E-Flux III cruise until near the end of April 2005. In particular, winds reached over 20 m s^{-1} during the first few days of the E-Flux III cruise, so that CTD sampling along Transect 1 (Table 3 and Figs. 12A and C) had to be curtailed because of the sea state. Thus, Transect 1 included only four CTD stations, but ADCP data were collected completely across it (see Table 3). During the remainder of the cruise, the winds were less than about 11 m s^{-1} for the most part, with a notable exception being a period when northwesterly winds ranged from 11 m s to over 17 m s^{-1} (~20 to over 30 knots) around March 16.

Cyclone *Opal* became visible in satellite SST (MODIS and GOES) imagery at approximately 20.00°N, 156.30°W to the southwest of the 'Alenuihaha Channel between about February 18 and 25 (Fig. 11B), but may have formed at least 1–2 weeks earlier. The genesis of Cyclone *Opal* was likely quite similar to that of Cyclone *Noah*, which formed at a location fairly close to *Noah*'s apparent origination position. Again, accelerated winds through the 'Alenuihaha Channel likely forced the eddy genesis. Lower wind speeds and warm-water "wakes" are apparent in the downwind shadows of Maui and Hawai'i, with cooler waters lying to the southwest of the 'Alenuihaha Channel

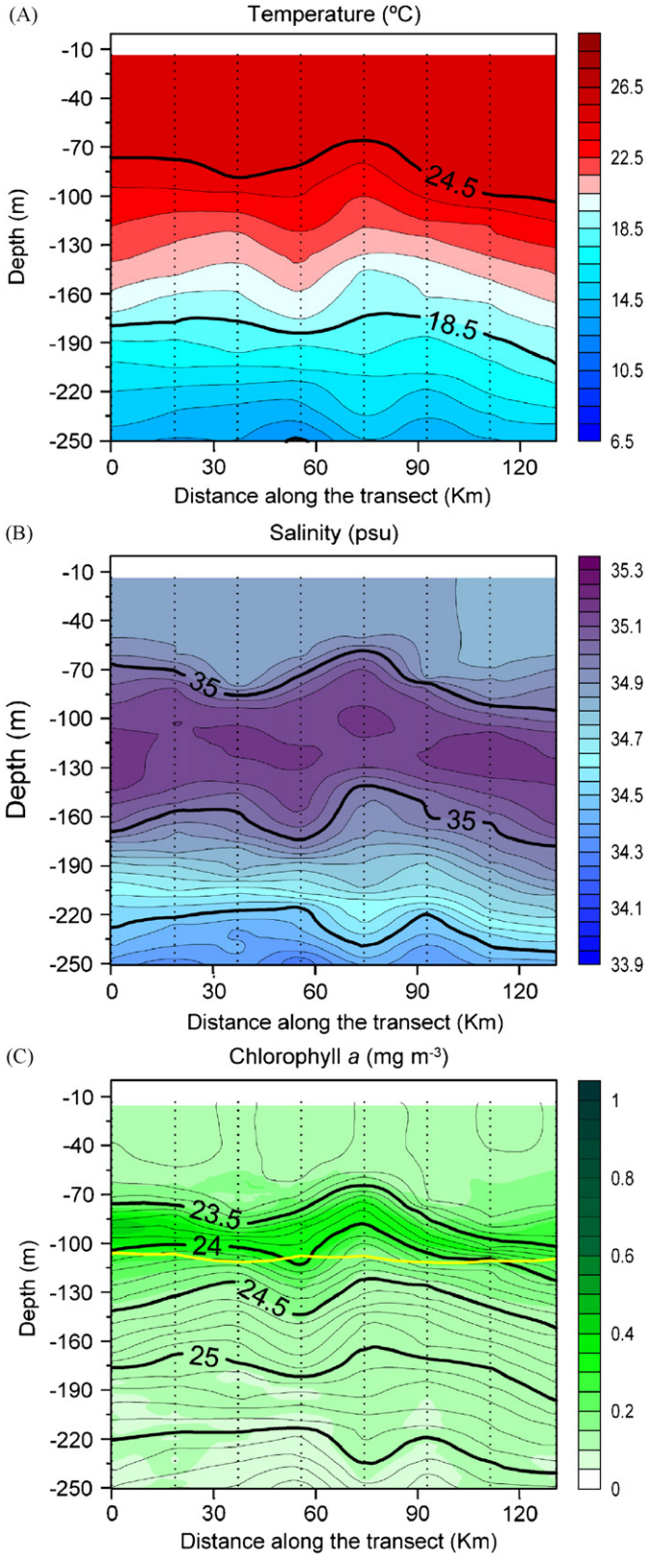

Fig. 9. Transect data for Transect 4 during E-Flux II. (A) Temperature (°C). (B) Nitrate + nitrite in color (μM). Isopycnal surfaces are shown with units of kg m^{-3}. (C) Chlorophyll *a* in color (mg m^{-3}). Isopycnal surfaces are shown with units of kg m^{-3}. Depth of the 1% light level is shown in yellow curve.

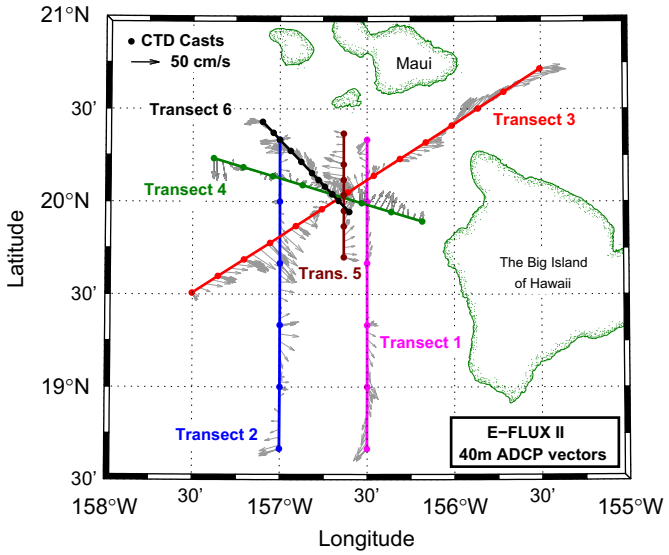

Fig. 10. ADCP current vectors in the upper layer (40 m) during E-Flux II.

(Figs. 11A–C). Cyclone *Opal* was evident in SST imagery until April 2005. As a reminder, the precise times of eddy formation and dissipation are only approximations. The E-Flux III R/V *Wecoma* cruise, conducted from March 10 to 28, 2005 (YD 69–87), thus may have occurred during the physically mature phase of the eddy.

Unlike Cyclone *Noah*, Cyclone *Opal* moved quite rapidly southward by about 160 km from the beginning to the end of the experiment with an overall average displacement speed of about 0.33 km h^{-1} (9.2 cm s^{-1}). The transit velocity of the eddy center varied considerably during the course of the experiment, at times being quite small while moving quite rapidly during others. For example, we estimate that during the period of March 11 and 12, when winds reached over 20 m s^{-1}, *Opal* moved southward at roughly 44 cm s^{-1} (slightly less than about 55 cm s^{-1}). This fast movement and the small scale (~40 km or less in diameter) of the eddy's inner-core region of extremely high biomass, productivity, and particle flux presented a major sampling challenge. The planned shipboard transect pattern (see Fig. 12A) was necessarily modified during the cruise in order to constrain all of the transects to pass through the center of the eddy. The data were then plotted and interpreted with respect to the moving center of the eddy in a quasi-Lagrangian reference frame (see Nencioli et al., 2008). A depiction of *Opal*'s movement in time and its approximate horizontal extent are illustrated in Fig. 12B. The actual sampling pattern for E-Flux III is shown in Fig. 12C. As mentioned earlier, careful monitoring of the underway ADCP data (using currents at a depth of about 40 m) was especially critical for tracking the center of *Opal* and planning of transects. ADCP current transects were also used to estimate the diameter of the eddy, which was found to be about 180–200 km; thus Cyclone *Opal*'s areal extent was much greater than that of the Island of Hawaii (Fig. 12B).

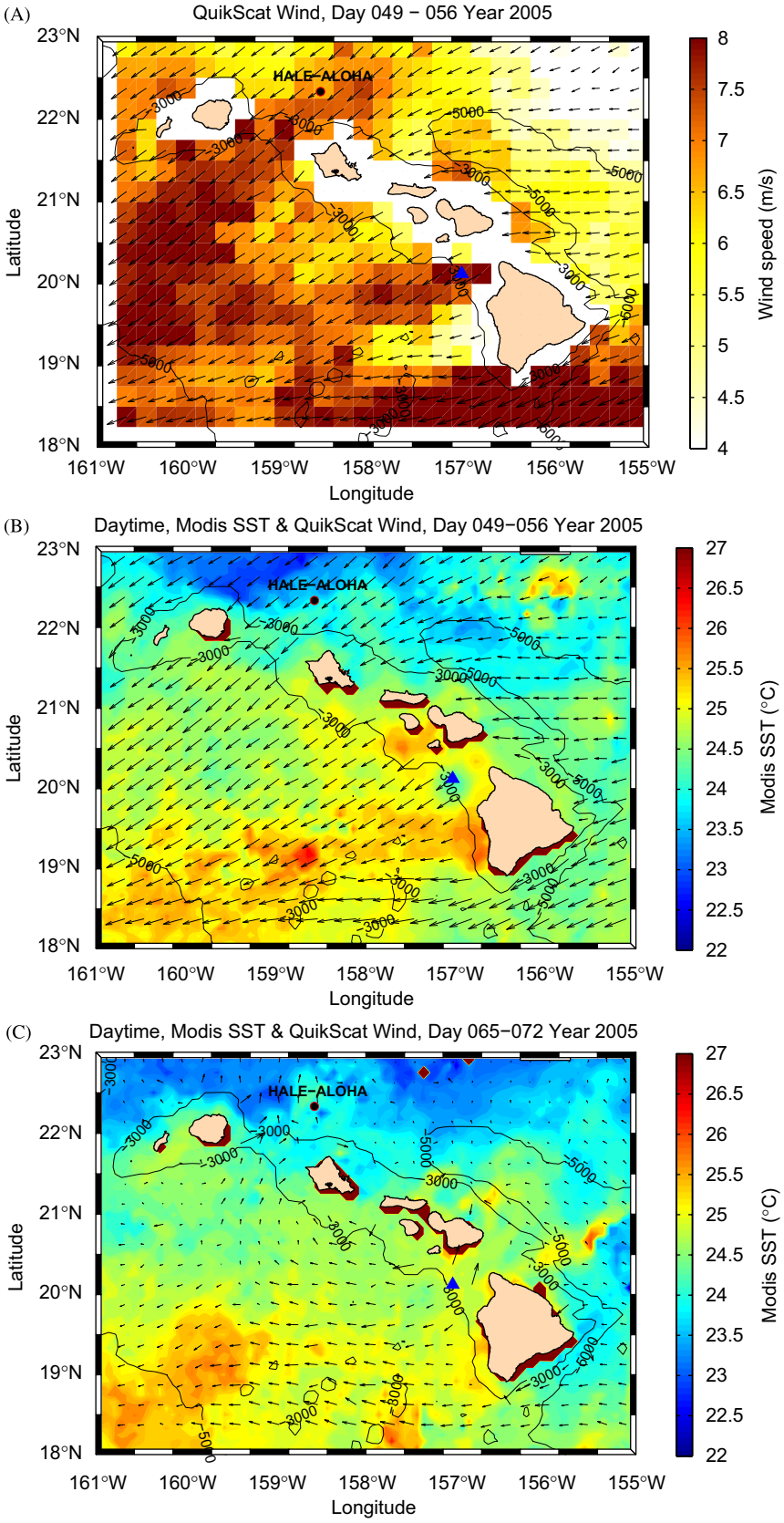

Fig. 11. (A) QuikScat wind vectors with wind speed magnitude shown in color prior to E-Flux III (February 18–25, 2005; YD 49–56). (B) MODIS sea-surface temperature in color and QuikScat wind vectors prior to E-Flux III (February 18–25, 2005; YD 49–56), and (C) during E-Flux I (March 6–13, 2005; YD 65–72). Blue triangles indicate location of time series of winds shown in Fig. 1.

Table 3
Dates and times (Hawaii Standard Time, local time) of the beginning and end of R/V *Wecoma* sampling operations during transects (see Fig. 12) and time series stations inside ("IN Stations") and outside ("OUT Stations') of E-Flux III

Operation	Beginning date (2005)	Beginning time (HST)	Ending date (2005)	Ending time (HST)
Transect 1	Mar. 10	2005	Mar. 11	1641
Transect 2	Mar. 11	2310	Mar. 12	1023
Transect 3*	Mar. 13	0200	Mar. 14	0600
Transect 4	Mar. 14	1415	Mar. 15	0705
Transect 5	Mar. 15	1050	Mar. 15	2158
Transect 6	Mar. 22	1355	Mar. 23	1025
IN Stations	Mar. 16	0040	Mar. 22	1000
OUT Stations	Mar. 23	2310	Mar. 27	1230

*Indicates the so-called "money run" transect which was the most intensively (more variables) sampled transect of the cruise.

Information concerning individual transects and stations within the eddy (IN-Stations) and outside the eddy (OUT-Stations) is summarized in Table 3. CTD/rosette sampling was done from near the surface to depths of 500, 1000, or 3000 m; Transect 3 was the most intensively sampled transect. The optics package also was deployed during some of the casts; however, discussion of these data is beyond the scope of this paper. The nominal spacing between stations was again about 16 km. Vertical transects of temperature, nitrate + nitrite concentrations, and chlorophyll *a* concentrations collected during Transect 3 of E-Flux III are shown in Fig. 13. We attempted to sample each section as rapidly as possible because of synopticity considerations and movement of the feature, but some error has been unavoidably introduced. From the density structure, it was possible to obtain a second estimate of the dimension of the eddy. The radial extent of the eddy was

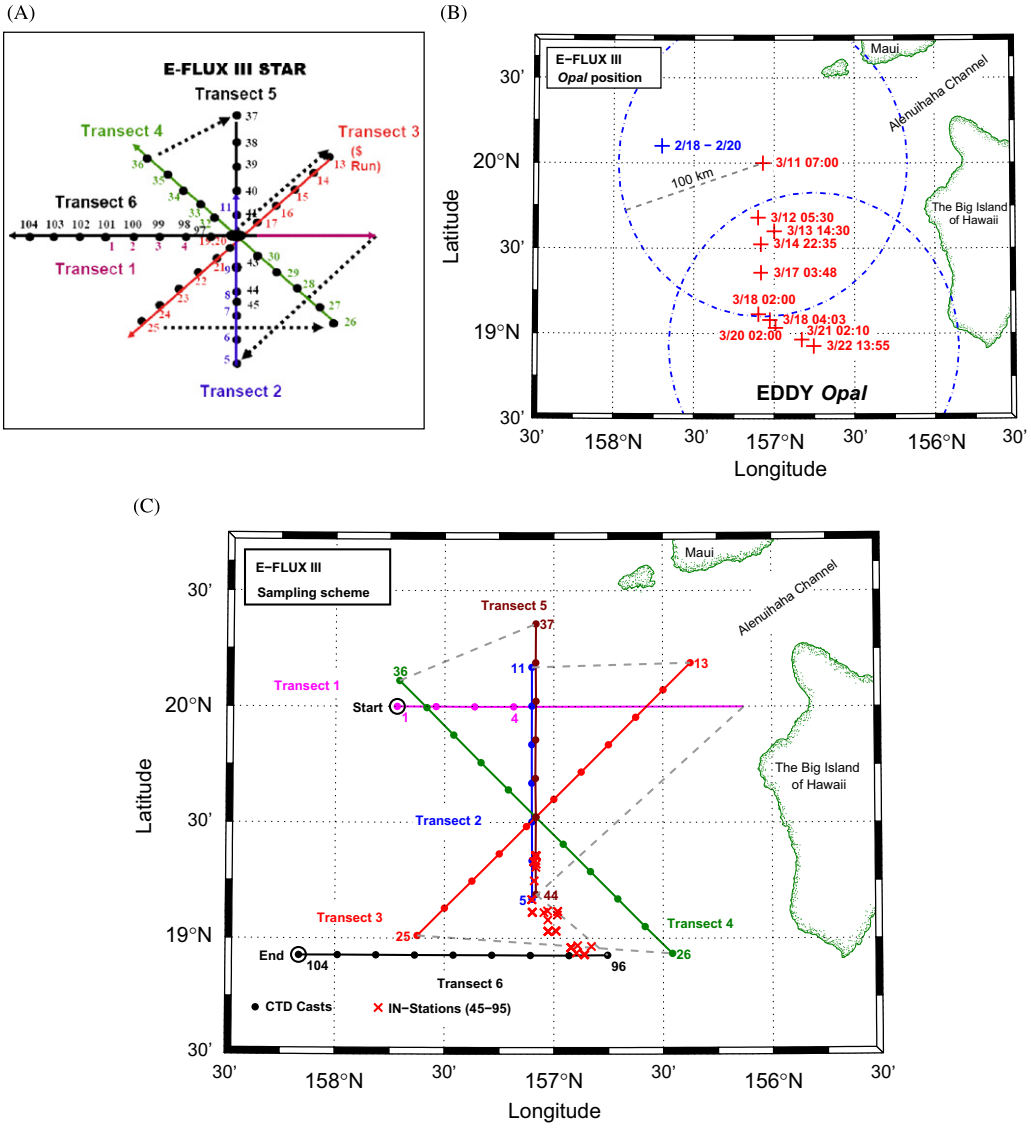

Fig. 12. (A) Planned sampling scheme for E-Flux III. (B) Rough dimensions of Eddy *Opal* and movement of the center of the eddy during E-Flux III. (C) Actual sampling scheme for E-Flux III.

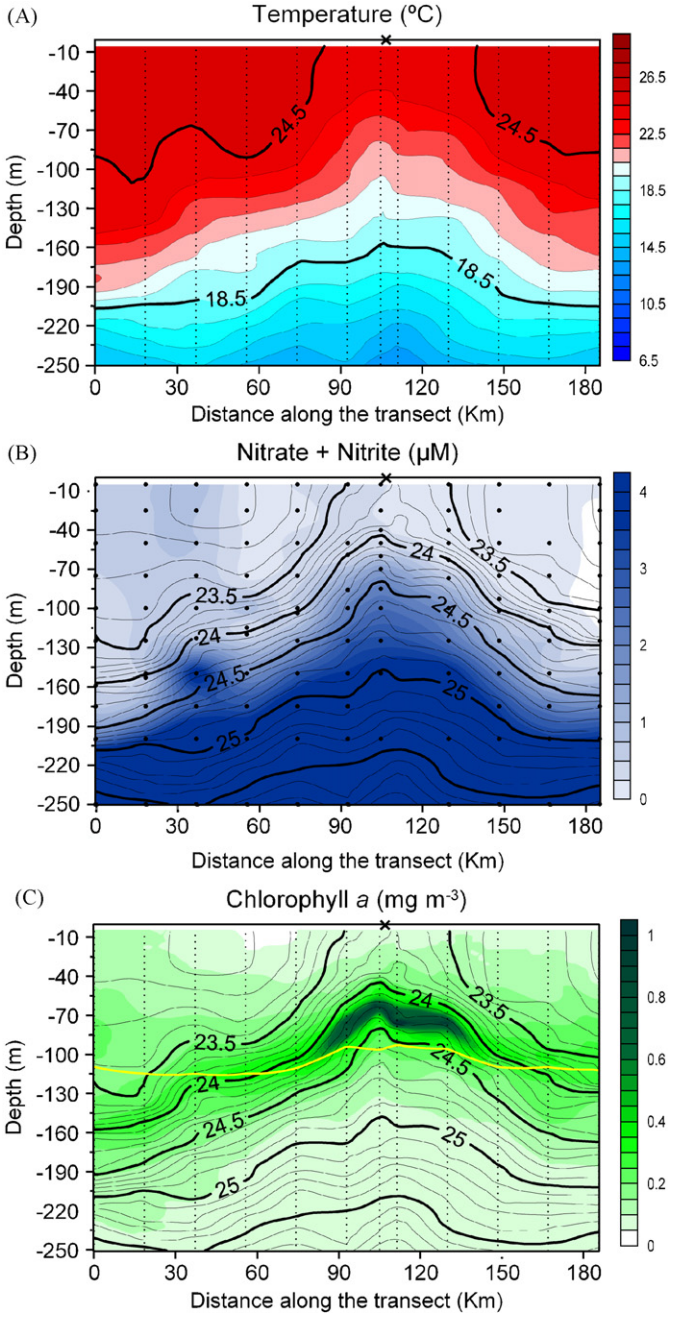

Fig. 13. Transect data for Transect 4 during E-Flux III. (A) Temperature (°C). (B) Nitrate + nitrite in color (μM). Isopycnal surfaces are shown with units of $kg\,m^{-3}$. (C) Chlorophyll *a* in color ($mg\,m^{-3}$). Isopycnal surfaces are shown with units of $kg\,m^{-3}$. Depth of the 1% light level is shown in yellow curve. The black X indicates the best-estimated position of the center of *Opal*.

defined to be at locations where isopycnal surfaces became nearly horizontal (i.e. where σ–$t = 24.0\,kg\,m^{-3}$ isopycnal reference surface or σ–t_{24} slopes were near zero), therefore we conservatively estimate the diameter of *Opal* to be 180–200 km. These values are in good agreement with the ones obtained from the 40-m ADCP data.

The most important information evident in the Transect 3 section data is reflected in the doming of isotherms, isopycnal surfaces, and isopleths of nitrate + nitrite and chlorophyll *a* toward the center of the eddy. The doming shows the classic structure of a cold-core eddy (Fig. 13). For example, isotherms at a depth of 150 m outside the eddy are uplifted toward the center by about 70 m with some isotherms within the eddy apparently outcropping to the surface. Outcropping of isopycnals (σ–$t = 23.2$, 23.4, and 23.6 $kg\,m^{-3}$) at the surface suggests that the eddy was intense and likely in a well-developed segment of its lifetime. Similarly, uplifting of the 35 psu isohaline surface near the eddy's center and outcropping of isohalines are evident in the data sets as well (note: salinity data are shown in Nencioli et al., 2008). A subsurface inner-core of high-salinity water is centered at a depth of about 75 m. Similarly, Fig. 13 shows a central chlorophyll *a* maximum peak characterized by concentrations greater than $1.5\,mg\,m^{-3}$ near the eddy's center, which is located at a depth of roughly 70 m. The chlorophyll *a* maximum layer deepens with increasing distance from the center of the eddy and chlorophyll *a* concentration decreases radially as well. The chlorophyll *a* maximum layer was well confined within a narrow band of isopycnal surfaces (σ–t surfaces of 24.1–24.3 $kg\,m^{-3}$), and there was a good correspondence between chlorophyll *a* and particulate maxima (not shown here). The inner-core region of high chlorophyll *a* was apparently less than 40 km in diameter. The 1% light level depth is also indicated in the chlorophyll *a* panel of Fig. 13. The uplifting of nutrients into the euphotic layer and the elevated chlorophyll *a* levels toward the center of the eddy are consistent with increased productivity produced by enhanced nutrient availability within cold-core eddies. The inner-core of the eddy shows strong anomalies reflected in lower temperature, higher salinity, greater density, higher nitrate + nitrite concentrations, and higher chlorophyll *a* concentrations (see figures in Nencioli et al., 2008).

The ADCP currents (40-m depth) for all of the E-Flux III cruise transects are displayed in Fig. 14. This depiction is in a quasi-Lagrangian reference frame. That is, the position of the eddy's center was estimated for each transect using 40-m ADCP data (see Nencioli et al., 2008); then all transects were translated to place their centers to be coincident with the center of Transect 3 (the "money run"). The cyclonic flow field is evident in Fig. 14, which shows near zero currents at the eddy's center and roughly linearly increasing tangential currents to their maximum values ($\sim 60\,cm\,s^{-1}$) at a radial distance of roughly 20–30 km. The horizontal currents then decrease radially. More information concerning currents, current shears, and vorticity is given in Nencioli et al., 2008). Fig. 15 shows the trajectory of the drifter deployed at the center of the eddy on March 13. Drifter data clearly show the cyclonic flow pattern of Cyclone *Opal*, as well as its southward migration. Several studies have focused on the propagation of Hawai'i lee eddies (Chassignet and Cushman-Roisin, 1991; Lumpkin, 1998; Holland and Mitchum, 2001). As mentioned earlier, Lumpkin (1998) reported that cyclonic eddies typically translate westward at near the wave speed of a first

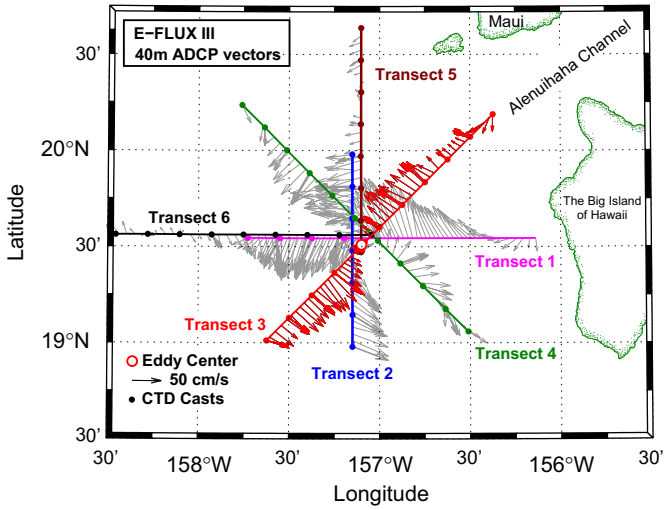

Fig. 14. ADCP current vectors in the upper layer (40 m) during E-Flux III. For every transect the position of the center of the eddy has been determined. The transects have been positioned with respect to the center of Transect 3.

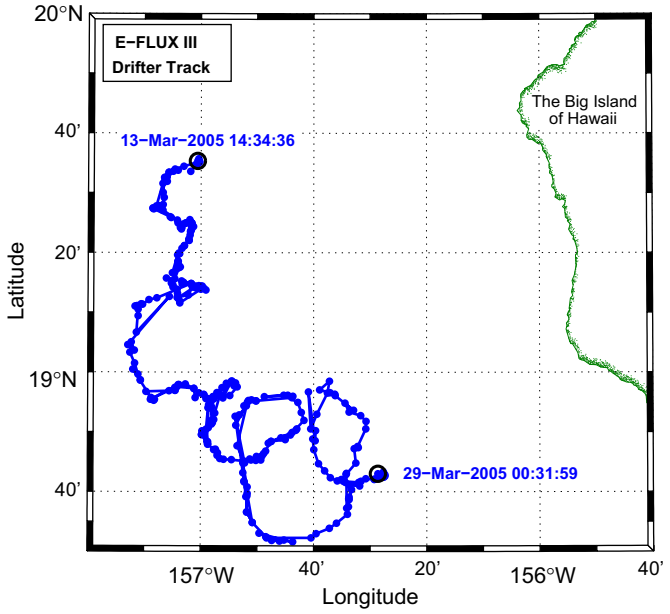

Fig. 15. Drifter trajectory during E-Flux III.

baroclinic Rossby wave. The southward movement of Cyclone *Opal* may be somewhat unusual and there are no obvious explanations for this observation. However, Patzert (1969) and Lumpkin (1998) also have reported cyclonic lee eddies which moved southward before translating west-northwestward. Also, a cyclonic lee eddy studied by Seki et al. (2002) during the 1995 Hawaiian Billfish Tournament, which began its formation in the 'Alenuihaha Channel, drifted to the southwest before moving eastward and impacting waters just off the west coast of Hawai'i. Thus, it is very difficult to generalize the results of studies of Hawaiian lee eddies, especially those concerning their propagation.

4. Discussion

Mesoscale eddies are formed via a variety of physical mechanisms and much has been learned about their roles in physical, biological, and biogeochemical processes since their discovery in the 1960s. However, these ubiquitous oceanic features have proven elusive for detailed study because of their ephemeral nature and limitations of in situ technologies. Specifically, eddies evolve and translate making them difficult to sample from ships. Satellites have proven to be highly effective at providing synoptic or quasi-synoptic views of the ocean's surface and near-surface features, but acquisition of information at depth still requires in situ measurements. Moorings have been valuable in studying the vertical structure of passing eddies, but subsurface horizontal spatial data are needed as well. Autonomous mobile platforms have not yet advanced to the point where sufficient instrumentation can be supported to comprehensively study eddies in situ. Thus, multi-platform approaches and modeling are clearly required for eddy studies (see review by Dickey and Bidigare, 2005). The E-Flux experiments were thus conducted at a time of evolving technologies.

Under the contemporary sampling constraints of the early 2000s, E-Flux investigators took advantage of past historical records and research that reported rather regular production of eddies in the lee of the Hawaiian Islands during trade wind conditions. We have examined wind time series in the vicinity of the Hawaiian Island chain from the QuikScat satellite scatterometer for the 1-year period of May 2004 through April 2005. During this period, trade wind (northeasterly) conditions were prevalent—occurring roughly 3/4 of the time. And during this same year-long period, at least three major cold-core cyclonic eddies were evident in SST satellite imagery to the southwest of the 'Alenuihaha Channel or to the west of the island of Hawai'i. These eddies had lifetimes that appear to have ranged from a bit more than a month (unnamed eddy of July 2004) to about four months (Cyclone *Noah* in 2004). We found that cold-core eddies were evident in satellite images for about 2/3 of the time during this 1-year period. Considering that SST and ocean-color satellite images reveal only eddies that have surface manifestations, it is quite possible that eddies were present during 3/4 or more of the year. Thus, the selection of our E-Flux study area to the west of Hawai'i was well justified. Our study suggests that this region could effectively serve as a viable "eddy testbed region" where novel, emerging ocean technologies could be utilized to improve our interdisciplinary knowledge of mesoscale eddies.

Why are eddies so regularly spawned in the E-Flux study region? A variety of mechanisms have been suggested to explain the presence of mesoscale eddies adjacent to islands (Lumpkin, 1998; review by Barton, 2001). The two leading candidates are current flow past islands and gradients in wind fields in the lee of islands. The former explanation appears to be quite plausible for some atolls, islands, or

island groups such as the Canary Islands (Barton et al., 2000, 1998). Flow past circular cylinders is a classic problem of fluid dynamics (Batchelor, 1967; Boyer, 1970). Using simple geometries for obstacles (i.e. cylinders) and homogeneous fluids, it has been shown that downstream disturbances or wakes take different forms that are dependent on a Reynolds number defined as $Re = Ud/v$ where U is the free upstream fluid velocity, d is the diameter of the cylinder (model island), and v is the kinematic viscosity of the fluid. Barton (2001) illustrates a progression of flows from laminar to attached eddies to attached eddies with unstable wakes with eddies to detaching eddies as Re increases from values less than 1 to greater than 80. For higher Reynolds numbers (say >80), vortex sheets essentially develop behind the cylinder. This simple model of wakes has several limitations if applied to the geophysical case of ocean islands. For example, (1) turbulence dominates the scales of flows of interest and thus eddy rather than molecular viscosities need to be invoked, (2) the geometries and shapes of islands and the surrounding bathymetry are complicated, (3) islands often occur in chains and interference of flows produced by each island can cause complex interactions, (4) bottom friction can become important, and (5) earth shape and rotational effects are generally non-negligible. Barton (2001) notes that observations of flow effects of islands based upon this mechanism have been generally unsuccessful because background or mean stream flows (values of U) have been too weak or variable or observations of the flows have been inadequate. Nonetheless, he cites evidence (computer model simulations) that eddies off the island of Barbados may have been spun up via ocean current flow disturbance by the island. For the E-Flux study, it appears unlikely that this particular mechanism is dominant for eddy production as the impinging flow is probably insufficient and the spacing of the islands is too close. Furthermore, the wind forcing mechanism, which is described next, seems to be overwhelmingly important based on previous and present results and analyses (Patzert, 1969; Lumpkin, 1998; Chavanne et al., 2002).Nonetheless, the Hawaiian island chain does play an important role on large-scale ocean circulation (Qiu et al., 1997; Xie et al., 2001; Chavanne et al., 2002), which is beyond the scope of this work.

The second mechanism for ocean eddy production in the environs of islands involves atmospheric wind flow perturbations by island mountains (Smith and Grubisic, 1993). At least three island chains appear to manifest this effect: the Hawaiian Islands, the Canary Islands, and the Cabo Verde Islands. Also, this phenomenon has been invoked to explain the formation of eddies off the west coast of Mexico where air is funneled through gaps in the Sierra Madre del Sur mountain range (Stumpf and Legeckis, 1977). Excellent detailed explanations for this mechanism are provided by Lumpkin (1998), Barton et al. (2000), and Chavanne et al. (2002). Hence we provide only a brief discussion of the mechanism as it applies to the E-Flux study area off the islands of Maui and Hawai'i. The topography introduced by the very tall mountains of Haleakala (3055 m or 10,023 ft) on Maui and Mauna Kea (4205 m or 13,796 ft) on Hawai'i serve as major obstacles for atmospheric flows, especially when winds are strong and steady (i.e. prevailing northeasterly trade wind conditions) and when an atmospheric inversion layer serves as a cap for the wind flow (Chen and Feng, 1995). Downstream of the islands, effective wind shear lines develop due to the wake effect with relatively stronger winds occurring through the 'Alenuihaha Channel and weaker winds in the wind shadows of the islands (Figs. 2A–C and 11A–C). Ekman transport in the ocean is proportional to the wind stress (roughly the square of the wind speed; i.e., Smith, 1988) according to the relations

$$S_x = \frac{\tau_y}{\rho f}, \quad S_y = -\frac{\tau_x}{\rho f} \tag{1}$$

where S_x and S_y (both in $\mathrm{m\,s^{-1}}$) are the eastward and northward components of the Ekman transport, τ_x and τ_y (both in $\mathrm{N\,m^{-2}}$) are the eastward and northward components of wind stress, ρ is the density of seawater ($\mathrm{kg\,m^{-3}}$), and f ($\mathrm{s^{-1}}$) is the local Coriolis parameter given by $f = 2\Omega \sin\theta$ where Ω is the Earth's rotation rate and θ is the latitude of the observations. The shear lines in wind speed thus result in strong gradients in Ekman transports (proportional to the wind speed squared) that are directed to the right of the wind vectors illustrated in Figs. 2A–C and 11A–C. The net effect is then to produce alternating patterns of upper ocean layer convergences and divergences downstream of the islands. In the converging zones, downwelling of near-surface water occurs whereas in diverging zones, upwelling of subsubsurface waters occurs. This condition sets the stage for the spin-up of cold-core mesoscale eddies and warm-core anti-cyclonic eddies as either relatively cool or relatively warm waters are isolated via flow instabilities and rotational effects. The spatial wind vector field distribution derived from QuikScat has been used to compute upwelling and downwelling velocity, w, via the Ekman pumping mechanism (Chavanne et al., 2002) according to

$$w = \frac{1}{\rho f}\left[\frac{\Delta\tau_y}{\Delta x} - \frac{\Delta\tau_x}{\Delta y}\right] \tag{2}$$

where w is in $\mathrm{m\,s^{-1}}$, and $\Delta\tau_y/\Delta x$ and $\Delta\tau_x/\Delta y$ are orthogonal gradients in wind stress. The final term in brackets in Eq. (2), $[\Delta\tau_y/\Delta x - \Delta\tau_x/\Delta y]$, is called the wind-stress curl, so local vertical velocity is proportional to the wind stress curl as both ρ and f are effectively constant for our case. Using the wind fields displayed in Figs. 2C, 7A, and 11C for E-Flux I, II, and III, respectively, we have computed the wind stress curl and Ekman pumping velocities, the latter shown in Figs. 16A–F. The wind-stress-curl field tends to take the form of dipole-like structures displaying positive values on the northern sides and negative values on the southern sides of the wind stress maxima. These lee effects often extend several island

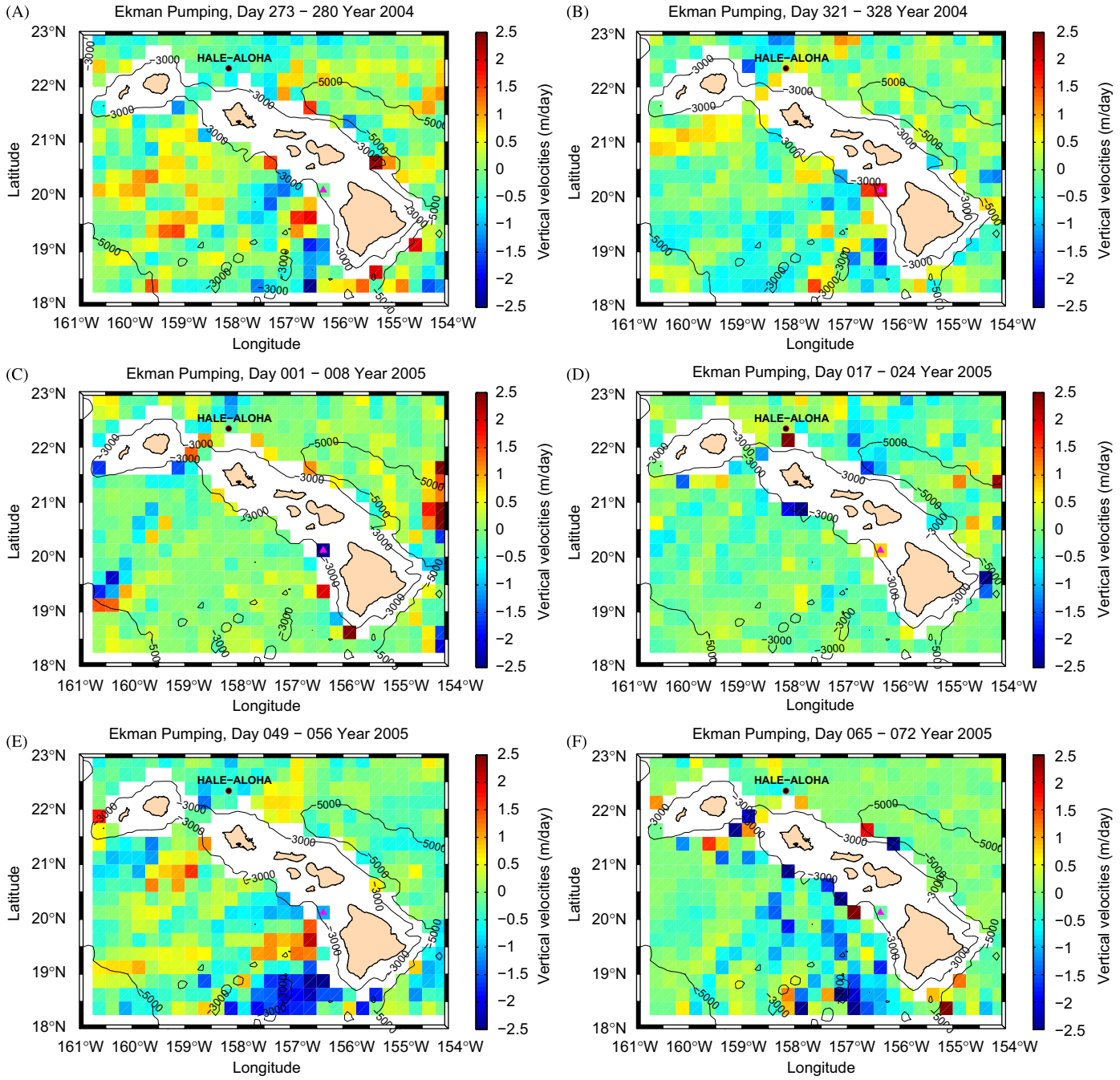

Fig. 16. Vertical velocities computed from wind-stress curl (Eq. (2)) using QuikScat data before (September 29–October 6, 2004; YD 273–280) and during (November 16–23, 2004; YD 321–328) E-Flux I, (A) and (B), E-Flux II (January 1–8, 2005; YD 1–8) and (January 17–24, 2005; YD 17–24), (C) and (D), and E-Flux III (February 18–25, 2005; YD 49–56) and (March 6–13, 2005; YD 65–72), (E) and (F). As expected, the upwelling velocities are much greater for E-Flux I and III than for E-Flux II.

diameter scales downwind as evidenced in SST images shown in Figs. 2B and C and 11B and C. Figs. 16A and E clearly show that during trade wind conditions (before E-Flux I and III), strong upwelling patterns occur with values reaching maximum values of roughly 1.5–2.5 m day^{-1} just downwind of the 'Alenuihaha Channel where we also see the formation of cyclonic eddies (i.e. Cyclone *Noah* during E-Flux I and Cyclone *Opal* during E-Flux III). These values are comparable to those reported in the same general oceanic region by Chavanne et al. (2002), who reported values of about 3 m day^{-1}. They commented that instantaneous values may well be higher and our coarse resolution of the wind field also would suggest that values presented here are likely lower limit estimates. Because of the Ekman pumping, the local thermoclines must necessarily be lifted in upwelling areas and depressed in downwelling zones. This effect likely contributes to the formation of cold-core cyclones and

warm-core anti-cyclones that are so often evident downstream of the Hawaiian Islands during persistent trade wind conditions. Note that the wind-stress-curl field and thus distribution of vertical velocities before and during E-Flux II (Figs. 16C and D) is rather featureless. This lack of wind shear, small wind-stress curl, and weak localized upwelling and downwelling velocities supports the argument that eddies are likely produced via the wind forcing mechanism rather than others such as oceanic flow. Calil et al. (2008) have recently done detailed numerical modeling simulations of the ocean response to realistic wind forcing in the lee of the Hawaiian Island chain, which are valuable for improving our understanding of the physical processes reported in our study. Also, Chavanne et al. (2002) did studies of wind forcing and oceanic responses for the Cabo Verde archipelago off the west coast of Africa.

Considerable research concerning island effects on ocean flows and biological processes has been conducted in the region of the Canary Islands (Barton, 2001; Aristegui et al., 1994, 1997; Barton et al., 2000, 2004; Basterretxea et al., 2002). The Canaries are high volcanic islands that are located where strong southwestward trade winds blow. The geophysical setting has several similarities to the Hawaiian Islands. Both the current flow and wind stress gradient mechanisms have been invoked to explain eddies in the wakes of the Canary Islands (Barton, 2001). One complication presented for Canary Island studies is the coastal effect of filaments that can interact with eddies (Barton et al., 2004). Nonetheless, comparative studies of physical and biological phenomena occurring in the Hawaiian, Canary, and Cabo Verde Islands should prove to be quite valuable, especially when model simulations can be done in conjunction with comprehensive field experiments.

5. Summary

The two major eddies that occurred to the west of Hawai'i during the period of May 2004 to April 2005 coincided with periods of strong trade winds. Cyclone *Noah* likely formed to the southwest of the 'Alenuihaha Channel in mid-August, over 2 1/2 months before the first E-Flux field experiment. Cyclone *Noah* appears to have formed shortly after another cold-core cyclone (unnamed) had drifted westward away from the 'Alenuihaha Channel area. Both of these features occurred during prolonged and strong trade wind conditions. The former unnamed eddy appears to have a lifetime of about 4–6 weeks whereas *Noah*, which existed for at least four months, was the longest-lived cyclone observed off Hawai'i during the study year. The E-Flux I field sampling began about three months after Noah's spin-up, indicating that the mature to perhaps decaying phase was observed. The strong currents ($\sim$80 cm s^{-1}) and well-developed doming of isotherms, isopycnals, nutrient isopleths, and chlorophyll *a* isopleths along with outcropping of some of the isopleths in the environs of the center of the eddy all suggest that *Noah* was still a well-developed and active eddy.

Following a hiatus of eddy activity from mid-December 2004 through early February 2005, Cyclone *Opal* appeared almost concurrently with the return of trade winds, which were not as steady as those that produced the first two cyclones of the year. However, there were strong pulses of trade winds during this period that may have reenergized Cyclone *Opal* and possibly contributed to its southward movement (i.e. possibly via induced inertial motions and Ekman transport) as observed in dramatic fashion during the ship-based sampling of E-Flux III. Like Cyclone *Noah*, Cyclone *Opal* displayed impressive upward doming of isotherms, isopycnal surfaces, chlorophyll *a* isopleths, and nutrient isopleths. Both cyclones also displayed inner-core regions of order of 10–30 km radius where chlorophyll *a* was elevated between two isopycnal surfaces. However, Cyclone *Opal* was nearly twice as large as Cyclone *Noah*. Nonetheless, both showed maximum tangential current speeds of about 60 cm s^{-1} in the upper 40 m of the water column. The E-Flux III cruise took place about 4–5 weeks following the spin-up of Cyclone *Opal*, which was very nearly circular, whereas the elliptically shaped Cyclone *Noah* was not observed by our ship-based sampling until about 2 1/2 months after its formation and likely at a later life-stage. Thus, it appears that we observed an earlier phase of evolution of a cyclone during E-Flux III. Other papers in this volume suggest that Cyclone *Opal* was decaying in terms of biological indicators (Brown et al., 2008; Landry et al., 2008a, b; Rii et al., 2008); however, during the cruise the physical parameters were relatively unchanged despite the eddy's relatively rapid southward movement. The lack of movement of Cyclone *Noah* and the rapid southward translation of Cyclone *Opal* are apparently unusual according the statistical analyses of multiple data sets by Lumpkin (1998), who suggested that cyclonic lee eddies typically move westward at near the speed of a first baroclinic mode Rossby wave.

Several strong correlations are evident between physical, chemical, and biological variables within the two cyclones that we studied. For example, isopleths of nutrients and chlorophyll *a* generally lie on isopycnal surfaces. That is, when isopycnal surfaces rise toward the centers of the eddies, so do isopleths of nutrients and chlorophyll *a*. This suggests that physics is controlling the availability of nutrients to the euphotic layer and that phytoplankton can thrive under these optimal conditions. Biological production and grazing rates, described in other papers in this volume (Brown et al., 2008; Landry et al., 2008a, b), certainly are important as well in regulating the concentrations of nutrients and chlorophyll within the eddy.

The estimation of upwelling velocities for eddy features is most difficult because of current technological limitations (i.e., few means are available to directly measure vertical velocities). Estimates based on rates of change of isopycnal surfaces are very problematic because our observations were done from a ship that was not

stationary, no moorings were available for the experiment, and slow mean vertical velocities were confounded with relatively energetic internal tides and internal gravity waves. The deduction of wind-induced vertical velocities using horizontal wind-stress-curl distributions does provide at least some order of magnitude estimates. However, spatial resolution of available satellite scatterometer data is insufficient to gain desired accuracy and spatial resolution. Clearly, models are sensitive to both good estimates of vertical and horizontal velocities for computing advection terms and estimates of turbulent diffusion. Unfortunately, no measurements of mixing, diffusion, or turbulence parameters were possible under the budgetary constraints of the E-Flux program. Nonetheless, Nencioli et al. (2008) have introduced some important ideas concerning nutrient inputs within Cyclone *Opal*, hypothesizing a conceptual model in which the eddy acts more like an open bottom/horizontally leaky feature, rather than like a closed system with no exchanges with the surrounding waters.

Despite many similar gross features and scales, each ocean eddy is unique. For example, there are several different genesis mechanisms for eddies that contribute to different physical, chemical, and biological distributions within their interiors. For example, Gulf Stream and Kuroshio eddies tend to retain materials derived from adjacent waters. On the other hand, materials found within Hawaiian lee eddies are likely locally produced suggesting that these eddies are likely more representative of gyre eddies. However, the subsurface expressions of the eddies studied during this experiment were relatively shallow, perhaps because they were rather newly formed. The Hawaiian lee eddies appear to go through several evolutionary stages and each translates along a unique path, presumably due to competing influences of the β-effects and flow conditions outside the eddy (i.e. in the atmosphere, hurricanes are steered by external wind patterns). There may well be eddy–eddy (vortex–vortex) interactions since cyclonic and anticyclonic eddies are often in close proximity in the lee of the Hawaiian Islands (Lumpkin, 1998). Such interactions would also likely affect the translations of the individual eddies. This aspect is considered in more detail for Cyclone *Opal* in the paper by Nencioli et al. (2008). It is clear that every eddy observation remains important for gaining new insights into processes, increasing our understanding, and developing and testing interdisciplinary models. Because we still have so few direct observations of eddies and the data we are presently able to collect are so limited in the number of key parameters and the spatial and temporal sampling, broad inferences and conclusions based on any single experiment or even a few such experiments must be considered in context. Future eddy research programs should be able to capitalize on emerging platform and sensor technologies as well as models using data assimilation and field programs using such models for adaptive sampling (Dickey and Bidigare, 2005). The region selected for the present study is ideal for such eddy studies.

Acknowledgments

We thank all of our E-Flux collaborators, particularly Claudia Benitez-Nelson, for their assistance in collecting the data described in this paper and for their intellectual contributions. Eric Firing and Jules Hammond provided expert assistance with the ADCP data sets. The crews and technicians of the R/V *KOK* and R/V *Wecoma* are thanked for their assistance at sea. The valuable comments and suggestions of anonymous reviewers are most appreciated as they significantly helped to strengthen the paper. This study was funded by the NSF Ocean Chemistry Program.

References

Allen, C.B., Kanda, J., Laws, E.A., 1996. New production and photosynthetic rates within and outside a cyclonic mesoscale eddy in the North Pacific subtropical gyre. Deep-Sea Research I 43, 917–936.

Alsdorf, D., Fu, L.L., Mognard, N., Cazenave, A., Rodriguez, E., Chelton, D., Lettenmaier, D., 2007. Measuring global oceans and terrestrial freshwater from space. EOS, Transaction of the American Geophysical Union 88 (24), 253–257.

Aristegui, J., Sangra, P., Henandez-Leon, S., Canton, M., Hernandez-Guerra, A., 1994. Island-induced eddies in the Canary Islands. Deep-Sea Research I 41, 1509–1525.

Aristegui, J., Tett, P., Hernandez-Guerra, A., Basterretxea, G., Montero, M.F., Wild, K., Sangra, P., Hernandez-Leon, S., Canton, M., Garcia-Braun, J.A., Pacheco, M., Barton, E.D., 1997. The influence of island-generated eddies on chlorophyll distribution: a study of mesoscale variation around Gran Canaria. Deep-Sea Research I 44, 71–96.

Barton, E.D., 2001. Island wakes. In: Steele, J.H., Thorpe, S.A., Turekian, K.K. (Eds.), Encyclopedia of Ocean Sciences, vol.5. Academic Press, Orlando, pp. 1397–1402.

Barton, E.D., Aristegui, J., Tett, P., Canton, M., Garcia-Braun, J., Hernandez-Leon, S., Nykjaer, L., Almeida, J., Almunia, J., Ballesteros, S., Basterretxea, G., Escanez, J., Garcia-Weill, L., Hernandez-Guerra, A., Lopez-Laatzen, F., Molina, R., Montero, M.F., Navarro-Perez, E., 1998. The transition zone of the Canary Current upwelling region. Progress in Oceanography 41, 455–504.

Barton, E.D., Basterretxea, G., Flament, P., Mitchelson-Jacob, E.G., Jones, B., Aristegui, J., Herrera, F., 2000. Lee region of Gran Canaria. Journal of Geophysical Research 105 (C7), 17173–17193.

Barton, E.D., Aristegui, J., Tett, P., Perez, E.N., 2004. Variability in the Canary Islands area of filament-eddy exchanges. Progress in Oceanography 62 (2–4), 71–94.

Basterretxea, G., Barton, E.D., Tett, P., Sangra, P., Navarro-Perez, E., Aristegui, J., 2002. Eddy and deep chlorophyl maximum response to wind-shear in the lee of Gran Canaria. Deep-Sea Research I 49 (6), 1087–1101.

Batchelor, G.K., 1967. An Introduction to Fluid Dynamics. Cambridge University Press, Cambridge.

Benitez-Nelson, C., Bidigare, R.R., Dickey, T.D., Landry, M.R., Leonard, C.L., Brown, S.L., Nencioli, F., Rii, Y.M., Maiti, K., Becker, J.W., Bibby, T.S., Black, W., Cai, W.J., Carlson, C.A., Chen, F., Kuwahara, V.S., Mahaffey, C., McAndrew, P.M., Quay, P.D., Rappe, M.S., Selph, K.E., Simmons, M.P., Yang, E.J., 2007. Mesoscale eddies drive increased silica export in the subtropical Pacific Ocean. Science 316, 1017–1020.

Bidigare, R.R., Benitez-Nelson, C., Leonard, C.L., Quay, P.D., Parsons, M.L., Foley, D.G., Seki, M.P., 2003. Influence of a cyclonic eddy on microheterotroph biomass and carbon export in the lee of Hawaii. Geophysical Research Letters 30 (6), 1318.

Boyer, D.L., 1970. Flow past a right circular cylinder in a rotating frame. Journal of Basic Engineering 92 (3), 430–436.

Brown, S.L., Landry, M.R., Selph, K.E., Yang, E.J., Rii, Y.M., Bidigare, R.R., 2008. Diatoms in the desert: plankton community response to a subtropical mesoscale eddy in the subtropical North Pacific. Deep-Sea Research II, this volume [doi:10.1016/j.dsr2.2008.02.012].

Calil, P.H.R., Richards, K.J., Jia, Y., Bidigare, R.R., 2008. Eddy activity in the lee of the Hawaiian Islands. Deep-Sea Research II, this volume [doi:10.1016/j.dsr2.2008.01.008].

Campbell, J.W., Blaisdell, J.M., Darzi, M., 1995. Level-3 SeaWiFS data products: spatial and temporal binning algorithms. NASA Technical Memorandum, Technical Report 104566, NASA Goddard Space Flight Center, Greenbelt, Maryland.

Chassignet, E.P., Cushman-Roisin, B., 1991. On the influence of a lower layer on the propagation of nonlinear oceanic eddies. Journal of Physical Oceanography 21 (7), 939–957.

Chavanne, C., Flament, P., Lumpkin, R., Dousset, B., Bentamy, A., 2002. Scatterometer observations of wind variations induced by oceanic islands: implications for wind-driven ocean circulation. Canadian Journal of Remote Sensing 28 (3), 466–474.

Chen, Y.L., Feng, J., 1995. The influences of inversion height on precipitation and air-flow over the island of Hawaii. Monthly Weather Review 123 (6), 1660–1676.

Cheney, R.E., Richardson, P.L., 1976. Observed decay of a cyclonic Gulf Stream ring. Deep-Sea Research 23 (2), 143–155.

Cushman-Roisin, B., Chassignet, E.P., Tang, B., 1990. Westward motion of mesoscale eddies. Journal of Physical Oceanography 20 (5), 758–768.

Dickey, T.D., Bidigare, R.R., 2005. Interdisciplinary oceanographic observations: the wave of the future. Scientia Marina 69 (Suppl. 1), 23–42.

Dickey, T.D., Granata, T., Marra, J., Langdon, C., Wiggert, J., Chai-Jochner, Z., Hamilton, M., Vasquez, J., Stramska, M., Bidigare, R.R., 1993. Seasonal variability of bio-optical and physical properties in the Sargasso Sea. Journal of Geophysical Research 98, 865–898.

Falkowski, P.G., Ziemann, D., Kolber, Z., Bienfang, P.K., 1991. Role of eddy pumping in enhancing primary production in the ocean. Nature 352, 55–58.

Fischer, A.S., Weller, R.A., Rudnick, D.L., Eriksen, C.C., Lee, C.M., Brink, K.H., Fox, C.A., Leben, R.R., 2002. Mesoscale eddies, coastal upwelling, and the upper-ocean heat budget in the Arabian Sea. Deep-Sea Research II 49 (12), 2231–2264.

Flierl, G.R., McGillicuddy, D.J., 2002. Mesoscale and submesoscale physical–biological interactions. In: Robinson, A.R., McCarthy, J.J., Rothschild, B. (Eds.), Biological–Physical Interactions in the Sea. The Sea, vol. 12. Wiley, New York, pp. 113–185 (Chapter 4).

Garcon, V., Oschlies, A., Doney, S.C., McGillicuddy, D.J., Waniek, J., 2001. The role of mesoscale variability on plankton dynamics in the North Atlantic. Deep-Sea Research II 48, 2199–2226.

Holland, C.L., Mitchum, G.T., 2001. Propagation of Big Island eddies. Journal of Geophysical Research 106 (C1), 935–944.

Honjo, S., Dymond, J., Prell, W., Ittekkot, V., 1999. Monsoon-controlled export fluxes to the interior of the Arabian Sea. Deep-Sea Research II 46 (8–9), 1859–1902.

Kuwahara, V.S., Nencioli, F., Dickey, T.D., Rii, Y.M., Bidigare, R.R., 2008. Physical dynamics and biological implications of cyclone Noah in the lee of Hawai'i during E-Flux I. Deep-Sea Research II, this volume [doi:10.1016/j.dsr2.2008.01.007].

Landry, M.R., Brown, K.E., Selph, K.E., Simmons, M.P., Rii, Y.M., 2008a. Depth-stratified phytoplankton dynamics in Cyclone Opal, a subtropical mesoscale eddy. Deep-Sea Research II, this volume [doi:10.1016/j.dsr2.2008.02.001].

Landry, M.R., Decima, M., Simmons, M.P., Hannides, C.C.S., Daniels, E., 2008b. Mesozooplankton biomass and grazing responses to Cyclone Opal, a subtropical mesoscale eddy. Deep-Sea Research II, this volume [doi:10.1016/j.dsr2.2008.01.005].

Leonard, C.L., Bidigare, R.R., Seki, M.P., Polovina, J.J., 2001. Interannual mesoscale physical and biological variability in the North Pacific Central Gyre. Progress in Oceanography 49 (1–4), 227–244.

Letelier, R.M., Karl, D.M., Abbott, M.R., Flament, P., Freilich, M., Lukas, R., Strub, T., 2000. Role of late winter mesoscale events in the biogeochemical variability of the upper water column of the North Pacific Subtropical Gyre. Journal of Geophysical Research 105 (C12), 28723–28739.

Lewis, M.R., 2007. Variability of plankton and plankton processes on the mesoscale. In: Williams, P.J.l.B., Thomas, D.N., Reynolds, C.S. (Eds.), Phytoplankton Productivity. Blackwell Science, Oxford, UK, pp. 141–155 (Chapter 6).

Lobel, P.S., Robinson, A.R., 1986. Transport and entrapment of fish larvae by ocean mesoscale eddies and currents in Hawaiian waters. Deep-Sea Research 33 (4), 483–500.

Lumpkin, C.F., 1998. Eddies and currents in the Hawaii islands. Ph.D. Thesis, University of Hawaii.

McGillicuddy, D.J., Robinson, A.R., 1997. Eddy-induced nutrient supply and new production in the Sargasso Sea. Deep-Sea Research I 44 (8), 1427–1450.

McGillicuddy, D.J., Robinson, A.R., Siegel, D.A., Jannasch, H.W., Johnson, R., Dickey, T.D., McNeil, J.D., Michaels, A.F., Knap, A.H., 1998. Influence of mesoscale eddies on new production in the Sargasso Sea. Nature 394, 263–266.

McNeil, J.D., Jannasch, H.W., Dickey, T.D., McGillicuddy, D.J., Brzezinski, M., Sakamoto, C.M., 1999. New chemical, bio-optical and physical observations of upper ocean response to the passage of a mesoscale eddy off Bermuda. Journal of Geophysical Research 104, 15537–15548.

Morel, A., 1988. Optical modeling of the upper ocean in relation to its biogenous matter content (Case I waters). Journal of Geophysical Research 93 (C9), 10749–10768.

Nencioli, F., Kuwahara, V.S., Dickey, T.D., Rii, Y.M., Bidigare, R.R., 2008. Physical dynamics and biological implications of a mesoscale eddy in the lee of Hawai'i: Cyclone Opal observations during E-Flux III. Deep-Sea Research II, this volume [doi:10.1016/j.dsr2.2008.02.003].

Olson, D.B., 1980. The physical oceanography of two rings observed by the Cyclonic Ring Experiment, Part II: dynamics. Journal of Physical Oceanography 10, 514–527.

Oschlies, A., 2001. Model-derived estimates of new production: new results point towards lower values. Deep-Sea Research II 48 (10), 2173–2197.

Oschlies, A., Garcon, V., 1998. Eddy-induced enhancement of primary production in a model of the North Atlantic Ocean. Nature 394, 266–269.

Patzert, W.C., 1969. Eddies in Hawaiian Islands. Technical Report HIG-69-8, Hawaii Institute of Geophysics, University of Hawaii.

Qiu, B., Koh, D.A., Lumpkin, C., Flament, P., 1997. Existence and formation mechanism of the North Hawaiian Ridge Current. Journal of Physical Oceanography 27, 431–444.

Richman, J.G., Wunsch, C., Hogg, N.G., 1977. Space and time scales of mesoscale motion in the western North Atlantic. Reviews of Geophysics 15 (4), 385–420.

Rii, Y.M., Brown, S.L., Nencioli, F., Kuwahara, V.S., Dickey, T.D., Karl, D.M., Bidigare, R.R., 2008. The transient oasis: nutrient-phytoplankton dynamics and particle export in Hawaiian lee cyclones. Deep-Sea Research II, this volume [doi:10.1016/j.dsr2.2008.01.013].

Sakamoto, C.M., Karl, D.M., Jannasch, H.W., Bidigare, R.R., Letelier, R.M., Walz, P.M., Ryan, J.P., Polito, P.S., Johnson, K.S., 2004. Influence of Rossby waves on nutrient dynamics and the plankton community structure in the North Pacific subtropical gyre. Journal of Geophysical Research 109 (C5).

Seki, M.P., Polovina, J.J., Brainard, R.E., Bidigare, R.R., Leonard, C.L., Foley, D.G., 2001. Biological enhancement at cyclonic eddies tracked with GOES thermal imagery in Hawaiian waters. Geophysical Research Letters 28 (8), 1583–1586.

Seki, M.P., Lumpkin, R., Flament, P., 2002. Hawaii cyclonic eddies and blue marlin catches: the case study of the 1995 Hawaiian International Billfish Tournament. Journal of Oceanography 58, 739–745.

Smith, R.B., Grubisic, V., 1993. Aerial observations of Hawaii's wake. Journal of Atmospheric Sciences 50 (22), 3728–3750.

Smith, S.D., 1988. Coefficients for sea-surface wind stress, heat-flux, and wind profiles as a function of wind-speed and temperature. Journal of Geophysical Research 93 (C12), 15467–15472.

Stumpf, H.G., Legeckis, R.V., 1977. Satellite-observations of mesoscale eddy dynamics in the eastern tropical Pacific Ocean. Journal of Physical Oceanography 7 (5), 648–658.

Taupier-Letage, I., Puillat, I., Millot, C., Raimbault, P., 2003. Biological response to mesoscale eddies in the Algerian Basin. Journal of Geophysical Research 108 (C8), 3245 [doi:10.1029/1999JC000117].

UNESCO, 1981. Tenth report of the Joint Panel on Oceanographic Tables and Standards. Technical Report, UNESCO Technical Papers in Marine Science.

Vaillancourt, R.D., Marra, J., Seki, M.P., Parsons, M.L., Bidigare, R.R., 2003. Impact of a cyclonic eddy on phytoplnkton community structure and photosynthetic competency in the subtropical North Pacific Ocean. Deep-Sea Research I 50, 829–847.

Xie, S.P., Liu, W.T., Liu, Q.Y., Nonaka, M., 2001. Far-reaching effects of the Hawaiian islands on the Pacific Ocean–atmosphere system. Science 292 (5524), 2057–2060.